1998

Recovery of the power spectrum of mass fluctuations from observations of the Ly alpha forest

RAC Croft

DH Weinberg

N Katz
University of Massachusetts - Amherst

L Hernquist

Recommended Citation
Croft, RAC; Weinberg, DH; Katz, N; and Hernquist, L, "Recovery of the power spectrum of mass fluctuations from observations of the Ly alpha forest" (1998). *ASTROPHYSICAL JOURNAL*. 366.
10.1086/305289

Recovery of the Power Spectrum of Mass Fluctuations from Observations of the Lyman-alpha Forest

Rupert A.C. Croft[1,5], David H. Weinberg[1,6], Neal Katz[2,7], and Lars Hernquist[3,4,8]

ABSTRACT

We present a method to recover the shape and amplitude of the power spectrum of mass fluctuations, $P(k)$, from observations of the high redshift Lyα forest. The method is motivated by the physical picture that has emerged from hydrodynamic cosmological simulations and related semi-analytic models, in which typical Lyα forest lines arise in a diffuse, continuous, fluctuating intergalactic medium. The thermal state of this low density gas ($\delta\rho/\rho \lesssim 10$) is governed by simple physical processes, which lead to a tight correlation between the Lyα optical depth and the underlying matter density. To recover the mass power spectrum, we (1) apply a monotonic Gaussian mapping to convert the QSO spectrum to an approximate line-of-sight density field with arbitrary normalization, (2) measure the power spectrum of this continuous density field and convert it to the equivalent 3-dimensional $P(k)$, and (3) evolve cosmological simulations with this $P(k)$ shape and a range of normalizations and choose the normalization for which the simulations reproduce the observed power spectrum of the transmitted QSO flux. Imposing the observed mean Lyα opacity as a constraint in step (3) makes the derived $P(k)$ normalization insensitive to the choice of cosmological parameters, ionizing background spectrum, or reionization history. Thus, in contrast to estimates of $P(k)$ from galaxy clustering, there are no uncertain "bias parameters" in the recovery of the mass power spectrum from the Lyα forest. We test the full recovery procedure on smoothed-particle hydrodynamics (SPH) simulations of three different cosmological models and show that it recovers the true mass power spectrum of the models on comoving scales $\sim 1-10h^{-1}$ Mpc, the upper scale being set by the size of the simulation boxes. The procedure works well even when it is applied to noisy (S/N$\sim$10), moderate resolution (~ 40 km s^{-1} pixels) spectra. We present an

[1]Department of Astronomy, The Ohio State University, Columbus, OH 43210

[2] Department of Physics and Astronomy, University of Massachusetts, Amherst, MA, 01003

[3]Lick Observatory, University of California, Santa Cruz, CA 95064

[4]Presidential Faculty Fellow

[5]racc@astronomy.ohio-state.edu

[6]dhw@astronomy.ohio-state.edu

[7]nsk@kestrel.phast.umass.edu

[8]lars@helios.ucolick.org

illustrative application to Songaila & Cowie's Keck HIRES spectrum of Q1422+231; the recovered $P(k)$ is consistent with that of an $\Omega = 1$, $h = 0.5$, $\sigma_8(z = 0) \approx 0.5$ cold dark matter model. The statistical uncertainty in this result is large because it is based on a single QSO, but the method can be applied to large samples of existing QSO spectra and should thereby yield the power spectrum of mass fluctuations on small and intermediate scales at redshifts $z \sim 2 - 4$.

Subject headings: quasars: absorption lines, Galaxies: formation, large scale structure of Universe

1. Introduction

A major goal of observational cosmology is the determination of the primordial power spectrum of mass fluctuations, $P(k)$. This spectrum is a direct prediction of theories of cosmic structure formation, and precise measurements of $P(k)$ would allow one to test these theories and constrain cosmological parameters, especially when combined with constraints from cosmic microwave background (CMB) anisotropies on very large scales. Most efforts to measure $P(k)$ have focused on galaxy redshift surveys. This route to the primordial power spectrum has several obstacles, including shot noise stemming from the discrete nature of the galaxy distribution and non-linear gravitational evolution of $P(k)$, which is important over much of the accessible range of scales. The most difficult problem to overcome is the uncertain relation between the galaxy and mass distributions, usually parametrized in terms of a (possibly scale-dependent) "bias factor" between the galaxy and mass power spectra. Furthermore, galaxy redshift surveys primarily probe structure at a single epoch, redshift zero. There are studies of clustering evolution, but the noise problems that afflict power spectrum measurements are even more severe in dilute, high redshift samples, and the evolution of bias is uncertain.

Recent theoretical models of the Lyα forest predict a tight, physically simple relation between the optical depth for Lyα absorption and the underlying mass density (Bi 1993; Bi, Ge, & Fang 1995; Reisenegger & Miralda-Escudé 1995; Bi & Davidsen 1997; Croft et al. 1997a; Hui, Gnedin, & Zhang 1997). This paper describes a method that exploits this tight relation to recover the mass power spectrum in the high redshift universe from QSO absorption spectra. We test the method using cosmological simulations and present an illustrative application to a single QSO spectrum (of Q1422+231).

Studies of the autocorrelation function of Lyα forest lines have shown little evidence for clustering on velocity scales $\Delta v \gtrsim 300$ km s^{-1} and only weak clustering on smaller scales (Cristiani et al. 1997 and references therein). Pando & Fang (1995), however, find significant large scale clustering in a power spectrum analysis of forest lines, using a technique based on wavelets.

Correlation analyses of metal line absorbers also show evidence for large scale clustering (Sargent, Boksenberg, & Steidel 1989; Heisler, Hogan, & White 1989; Quashnock, Vanden Berk, & York 1996; Quashnock & Vanden Berk 1997). The approach we take in this paper differs from these earlier studies in several respects. First, we work directly with the observed flux instead of with lines identified from it (as in the autocorrelation analyses of Press & Rybicki [1993] and Zuo & Bond [1994], though we focus on the power spectrum rather than the autocorrelation function). This approach has the advantage of reducing shot noise, as information in the continuous QSO spectrum is not condensed into a relatively small set of discrete numbers (line redshifts). It also circumvents ambiguities associated with line-identification algorithms, and it can be applied to spectra that have insufficient spectral resolution and/or signal-to-noise ratio for secure line identification. Equally important, we show how to recover the *amplitude* of the mass power spectrum from our measurements. The power spectrum of lines would be related to this quantity by an uncertain, and probably model dependent, "bias factor" of forest lines.

Our method is motivated by and relies upon the physical picture of the Lyα forest that has emerged from hydrodynamic simulations of cosmic structure formation (Cen et al. 1994; Zhang, Anninos, & Norman 1995; Hernquist et al. 1996; Wadsley & Bond 1996) and related analytic models of the intergalactic medium (Bi 1993; Bi, Ge, & Fang 1995; Reisenegger & Miralda-Escudé 1995; Hui et al. 1997; Bi & Davidsen 1997). In this picture, the Lyα forest arises in highly photoionized gas with density typically between 0.1 and 10 times the cosmic mean. For most of the gas in this density regime, the Lyα optical depth obeys the approximate relation $\tau \propto n_{\rm HI} \propto \rho_b^2 T^{-0.7}$, where $n_{\rm HI}$ is the density of neutral hydrogen, T is the temperature of the gas, and ρ_b is the local baryon density. Baryons trace the dark matter in this density regime, and the interplay between cooling by the expansion of the universe and heating by photoionization leads to a simple, tight relation between gas density and temperature (Croft et al. 1997a; Hui & Gnedin 1997). Thus, to a good approximation, the optical depth satisfies $\tau \propto \rho^\beta$, with $\beta \sim 1.5 - 2$. This discussion ignores the effects of peculiar velocities, thermal broadening, shock heating, and collisional ionization, but simulations with all of these effects included retain the tight relation between τ and ρ (see figure 2 of Croft et al. 1997a).

The transmitted flux in a QSO spectrum, $F = e^{-\tau}$, is monotonically related to ρ in this approximation. Fluctuations in the density field along the line of sight to the QSO produce fluctuations in the absorption, which are seen as the Lyα forest. Because the relation between τ and ρ is fairly simple, one can extract information about the underlying mass density field from the observed flux distribution. One approach would be to invert the above relations, deriving τ from F and ρ from τ. However, the mapping between ρ and F is non-linear (an exponential of a power law), and it depends on the unknown constant of proportionality in the $\tau - \rho$ relation. Also, it is difficult to measure τ accurately in saturated regions, where $F \simeq 0$.

Rather than attempt a direct inversion, in this paper we use the fact that the primordial density field is expected to have a Gaussian probability distribution function (PDF), at least in inflationary models for the origin of fluctuations. We monotonically map the flux in a QSO

spectrum back to a Gaussian density field, as in Weinberg's (1992) method for recovering primordial fluctuations from the observed galaxy distribution. We measure the 1-dimensional power spectrum $P_{\rm 1D}(k)$ of this Gaussian density field and convert it to the equivalent 3-dimensional $P(k)$. At this point we have the shape of the initial mass $P(k)$, but since the variance of the Gaussian PDF is not yet known, we have no information about its amplitude. To normalize $P(k)$ we evolve an N-body simulation using Gaussian fluctuations with the derived $P(k)$ for the initial conditions. We then use the temperature–density relation to generate QSO spectra from this simulation, choosing the photoionization rate to reproduce the observed mean Lyα opacity. The amplitude of the *flux* power spectrum depends almost exclusively on the amplitude of the mass $P(k)$. Therefore, when the amplitude of the flux power spectrum in the simulated spectra matches that measured from the observations, the underlying mass $P(k)$ has the correct amplitude. We then have the normalized $P(k)$ of linear mass fluctuations at the redshift probed by the QSO spectrum.

Obviously, there are many assumptions and approximations involved in the procedure outlined above, and it is not obvious a priori that it will work. Most of this paper will be devoted to testing these assumptions and the method as a whole. In §2 we explain the method for recovering $P(k)$ in more detail, testing the steps of the procedure individually. In §3 we test the procedure as a whole by attempting to recover the mass power spectrum from simulated observational spectra extracted from hydrodynamic simulations of different cosmological models. In §4 we apply the method to the spectrum of QSO Q1422+231 (provided by A. Songaila and L. Cowie). In §5 we summarize our results and outline directions for future investigation.

2. Method

2.1. Numerical simulations and physical motivation

QSO spectra extracted from hydrodynamic cosmological simulations will play the role of simulated observations, against which we test our procedure. With these simulated spectra, we can control the physical and "instrumental" effects incorporated and test their influence in isolation, and we know the true mass power spectrum that the method should recover. As already mentioned, our method for recovering $P(k)$ presumes the basic picture of the Lyα forest that emerges from these simulations, and our tests in this paper depend on its validity. We will briefly mention tests of the scenario itself in §5.

Our simulations use the N-body plus smoothed-particle hydrodynamics (SPH) code TreeSPH (Hernquist & Katz 1989; Katz, Weinberg, & Hernquist 1996). We consider three different cold dark matter (CDM) cosmological models; the simulations are the same ones analyzed by Croft et al. (1997a), and we refer the reader to that paper for details beyond those given here. The first model is "standard" CDM (SCDM), with $\Omega = 1$, $h = 0.5$ (where $h \equiv H_0/100$ km s^{-1} Mpc^{-1}). The power spectrum is normalized so that the rms amplitude of mass fluctuations in 8 h^{-1}Mpc

spheres, linearly extrapolated to $z = 0$, is $\sigma_8 = 0.7$. This normalization is consistent with that advocated by White, Efstathiou, & Frenk (1993) to match the observed masses of rich galaxy clusters, but it is inconsistent with the normalization implied by the COBE-DMR experiment. Our second model is identical to the first except that $\sigma_8 = 1.2$. This higher amplitude is consistent with the 4-year COBE data (Bennett et al. 1996), and we therefore label the model CCDM. The third model, OCDM, assumes an open universe with $\Omega_0 = 0.4$, $h = 0.65$. This model is also COBE-normalized, with $\sigma_8 = 0.75$ (Ratra et al. 1997). The baryon density parameter for all of these models is $\Omega_b = 0.0125h^{-2}$, a value taken from Walker et al. (1991).

We simulate one periodic cube of side length 11.111 h^{-1}Mpc for each model, using 64^3 collisionless dark matter particles and 64^3 gas particles. Each simulation was evolved to $z = 2$. We will deal exclusively with the $z = 3$ outputs in this paper. A uniform photoionization field was imposed and radiative cooling and heating rates calculated assuming optically thin gas, as described in Katz et al. (1996). QSO absorption spectra were extracted from lines of sight through the simulation outputs as described in Hernquist et al. (1996) and Croft et al. (1997a).

The simulated spectra exhibit a tight relation between the Lyα optical depth, τ, and the underlying baryon density, ρ_b, for $(\rho_b/\overline{\rho}_b) \lesssim 10$. This relation arises because the temperature of the low density gas is determined by the interplay between photoionization heating by the UV background and adiabatic cooling by the expansion of the universe, leading to a simple temperature–density relation that is well approximated by a power law,

$$T = T_0(\rho_b/\overline{\rho}_b)^{\alpha}. \tag{1}$$

The constants T_0 and α depend on the spectral shape of the UV background and on the history of reionization; they are likely to lie in the ranges 4000 K $\lesssim T_0 \lesssim$ 15,000 K and $0.3 \lesssim \alpha \lesssim 0.6$ (see Hui & Gnedin 1997). The Lyα optical depth is proportional to the neutral hydrogen density $n_{\rm HI}$ (Gunn & Peterson 1965), which for gas in photoionization equilibrium is proportional to the density multiplied by the recombination rate. For temperatures $T \sim 10^4$ K, the combination of these effects yields

$$\tau \propto \rho_b^2 T^{-0.7} = A(\rho_b/\overline{\rho}_b)^{\beta}, \tag{2}$$
$$A = 0.946 \left(\tfrac{1+z}{4}\right)^6 \left(\tfrac{\Omega_b h^2}{0.0125}\right)^2 \left(\tfrac{T_0}{10^4\ {\rm K}}\right)^{-0.7} \left(\tfrac{\Gamma}{10^{-12}\ {\rm s}^{-1}}\right)^{-1} \left(\tfrac{H(z)}{100\ {\rm km\ s^{-1}\ Mpc^{-1}}}\right)^{-1},$$

with $\beta \equiv 2 - 0.7\alpha$ in the range $1.6 - 1.8$. Here Γ is the HI photoionization rate, and $H(z)$ is the Hubble constant at redshift z. In this paper we will treat the (observationally uncertain) quantity Γ as a free parameter, which we set by requiring that our simulated spectra match the observed mean Lyα flux decrement at $z = 3$, $D_A \equiv 1 - \langle F \rangle = 0.36$ (Press, Rybicki, & Schneider 1993; Rauch et al. 1997; but see Zuo & Lu 1993, who estimate a lower mean decrement). If we adopted a different baryon density or reionization history in the simulations then the required value of Γ would be different. As equation (2) suggests, in a given cosmological model the mean flux decrement basically constrains the parameter combination $\Omega_b^2 \Gamma^{-1} T_0^{-0.7}$, and for a fixed value

of this combination one gets nearly identical spectra from an underlying density field, whatever the individual values of the parameters.

The optical depth depends on the density of neutral atoms in redshift space rather than in real space, so peculiar velocities and (to a lesser extent) thermal broadening introduce scatter in the relation between τ and ρ_b. Equation (2) breaks down more drastically in regions with $(\rho_b/\overline{\rho}_b) \gtrsim 10$ because of shock heating and collisional ionization, but these regions have a small volume filling factor so they affect only a small fraction of a typical spectrum. As shown in figure 2 of Croft et al. (1997a), the correlation between τ and ρ_b remains tight over most of the spectrum even when all of the relevant physical effects are taken into account. Finally, because the gaseous structures responsible for typical Lyα forest lines are large ($\gtrsim 100$ kpc), low density, and fairly cool ($T \sim 10^4$ K), pressure gradients have only a small effect on their dynamics relative to gravity, and the gas within them traces the underlying dark matter except on very small scales. Equation (2) therefore provides a link between the Lyα optical depth and the total mass density $\rho = (\Omega/\Omega_b)\rho_b$. We will show below that, as a result of this link, the power spectrum of the flux has the same shape as the power spectrum of the underlying mass fluctuations on large scales.

2.2. Recovery of the power spectrum shape

Given the relation between optical depth and density, we would like to recover the density field along the line of sight and measure its power spectrum. We could attempt to recover ρ by inverting equation (2), but we would encounter several obstacles. In high density regions the QSO spectrum saturates, and when $F \approx 0$ it is difficult to measure $\tau = -\ln F$ accurately. Since the power spectrum weights high amplitude regions strongly (the galaxy power spectrum, for instance, is strongly affected by galaxies in rich clusters even though field galaxies are much more common), small amounts of noise in saturated regions could produce large uncertainties in the power spectrum of the recovered density field. Obtaining ρ by direct inversion also requires a priori knowledge of the proportionality constant A in equation (2). A given spectrum could potentially be produced either by a weakly fluctuating density field with a large value of A or by a strongly fluctuating density field with a small value of A. Since the $\tau - \rho$ relation is non-linear, changes in A are not equivalent to linear rescalings of $P(k)$. When we extract spectra from simulations, we fix A by matching the observed mean flux decrement, but we are able to do so only because the simulation itself provides the density field. Finally, from the point of view of testing cosmological models, we are interested primarily in the power spectrum of the initial, linear mass fluctuations, rather than the power spectrum of the non-linear density field. At large scales and high redshifts, non-linear evolution has little effect on $P(k)$, and the linear and non-linear power spectra can be related by analytic approximations (Hamilton et al. 1991; Peacock & Dodds 1996; Jain, Mo, & White 1995) or by numerical calculations. However, to the extent that we can recover the linear $P(k)$ directly from the observations, we are somewhat closer to our ultimate goal of addressing cosmological questions.

We can circumvent all of these obstacles — saturation, the unknown value of A, and non-linear evolution of the density field — using "Gaussianization," a technique introduced by Weinberg (1992) as a tool for recovering primordial density fluctuations from the observed galaxy distribution. Inflationary models for the origin of structure predict that the initial density field has a Gaussian PDF. Gravitational evolution skews the PDF, but it tends to carry high density regions of the initial conditions into high density regions of the evolved density field, low density regions into low density regions, and so on in between; it therefore preserves an approximately monotonic relation between initial and final density even on scales that are moderately non-linear. Given an evolved density field on a grid, one can recover an approximate map of the initial fluctuations by sorting the pixels in order of density and then assigning new densities to the pixels so that they have the same rank order but a Gaussian PDF. The overall amplitude of the fluctuations, corresponding to the width of the Gaussian, must be determined in a separate step, by evolving the recovered initial conditions and comparing them to the observations.

In the application described by Weinberg (1992), the input data set is a galaxy density field from a redshift survey. In our case we will apply Gaussianization to Lyα forest spectra, where the physical discussion in §2.1 gives us excellent reason to expect a monotonic relation between observed flux and mass density, approximately $F = \exp[-A(\rho/\overline{\rho})^{\beta}]$. Because Gaussianization uses only the rank order of the pixel densities, we do not need to know the parameters of this non-linear relation, only that it is monotonic. An individual spectrum yields only a 1-dimensional probe through the density field, but we aim to recover the power spectrum of fluctuations rather than the full density field. Peculiar velocities can depress the power spectrum on small scales by smoothing structure in redshift space and adding scatter to the $\tau - \rho$ relation. However, on large scales they should not alter the shape of $P(k)$. Coherent flows into high density regions and out of low density regions can amplify the redshift-space power spectrum (Kaiser 1987), but our normalization procedure (described in §2.3 below) will automatically account for this effect.

Figure 1 illustrates the Gaussianization procedure for a sample spectrum taken from our SCDM model. The transmitted flux F (normalized to $F = 1$ for no absorption) is computed along a random line of sight through the simulation. The observed wavelength is related to the velocity by $\lambda = \lambda_\alpha(1+z)(1+v/c)$, where $\lambda_\alpha = 1216\mathring{A}$ is the Lyα rest wavelength and $z = 3$. The velocity range $\Delta v = 2222$ km s^{-1} ($\Delta z = 0.0296$) is set by the size of the periodic simulation box; a simulated spectrum like that in Figure 1a corresponds to a small section of an observed QSO spectrum. We have added noise to the spectrum (S/N=50 in the unabsorbed regions) in a manner described in §2.4 below. Figure 1b shows the PDF of the flux for 100 simulated spectra. This PDF is mapped by Gaussianization to the Gaussian PDF of the density contrast, $P(\delta)$, shown in Figure 1c. Figure 1d shows the line-of-sight density contrast field $\delta(v)$ inferred from the spectrum. This field is equivalent to the "initial" density contrast, in the sense that the fluctuations are Gaussian instead of having a PDF skewed by gravitational evolution. The amplitude of the field is arbitrary at this stage, and will be determined by a separate normalization process (described in §2.3). Noise in the spectrum causes the small scale spikiness seen in the recovered density contrast

field, especially in the lowest and highest density regions. Smoothing the spectrum over a few pixels prior to Gaussianization would suppress the noise and remove this spikiness, but we have not incorporated such smoothing in our analysis because we find that the noise does not change the derived power spectrum on the scales where our recovery method is reliable.

Now that we have an approximation to the initial mass density field along the line of sight, we would like to measure the 3-dimensional power spectrum, $P(k)$. We first estimate the 1-dimensional power spectrum, $P_{\rm 1D}(k) = \langle \delta^2(k) \rangle$, where

$$\delta(k) = \frac{1}{2\pi} \int \delta(x) e^{-ikx} dx. \tag{3}$$

For the simulated spectra, we compute $\delta^2(k)$ using a Fast Fourier Transform, then average over multiple lines of sight to find $P_{\rm 1D}(k)$. When we analyze the spectrum of Q1422+231 in §4, we will average over bins in k rather than multiple lines of sight. The 1-dimensional power spectrum $P_{\rm 1D}(k)$ is related to the 3-dimensional power spectrum $P(k)$ by

$$P_{\rm 1D}(k) = \frac{1}{2\pi} \int_k^\infty P(y) y dy \tag{4}$$

(Kaiser & Peacock 1991). Equation (4) shows that the 1-dimensional power spectrum on large scales receives contributions from 3-dimensional fluctuations at all smaller scales (higher k). Because of this aliasing of power, the 1-dimensional power spectra of pencil beam galaxy redshift surveys can sometimes show spurious large scale features that are not present in the 3-dimensional power spectrum (Kaiser & Peacock 1991; Baugh 1996). In order to recover $P(k)$ from $P_{\rm 1D}(k)$, one must invert equation (4),

$$P(k) = -\frac{2\pi}{k} \frac{d}{dk} P_{\rm 1D}(k). \tag{5}$$

The dilute sampling in pencil beam galaxy surveys can make such an inversion noisy, but in our case we start from a continuous spectrum instead of a discrete distribution of objects, and the inversion (5) proves quite practical even given realistic levels of observational noise.

Figure 2 illustrates the recovery of the shape of $P(k)$ from 100 spectra drawn from the SCDM simulation at $z = 3$. We did not add noise to these spectra; we will examine the effects of noise and instrumental resolution in §2.4 below. Filled circles represent the 3-dimensional $P(k)$ recovered from the Gaussianized spectra. The normalization has been chosen to match the amplitude of the linear theory SCDM mass power spectrum at $z = 3$, shown by the solid curve. Open circles show the 3-dimensional $P(k)$ recovered directly from the flux, without Gaussianization, again normalized to match the linear theory mass power spectrum at large scales.

The power spectrum derived from the Gaussianized flux matches the shape of the linear theory $P(k)$ quite well for comoving wavelengths $\lambda = 2\pi/k \gtrsim 1.5\ h^{-1}$Mpc, up to the scale of the simulation box, $\lambda = 11.111\ h^{-1}$Mpc. The redshift path length of the Lyα forest region for a $z = 3$ QSO corresponds to roughly 20 of our simulated spectra. We have therefore divided our 100 Gaussianized spectra into five sets of 20 and computed $P(k)$ separately for each set. The

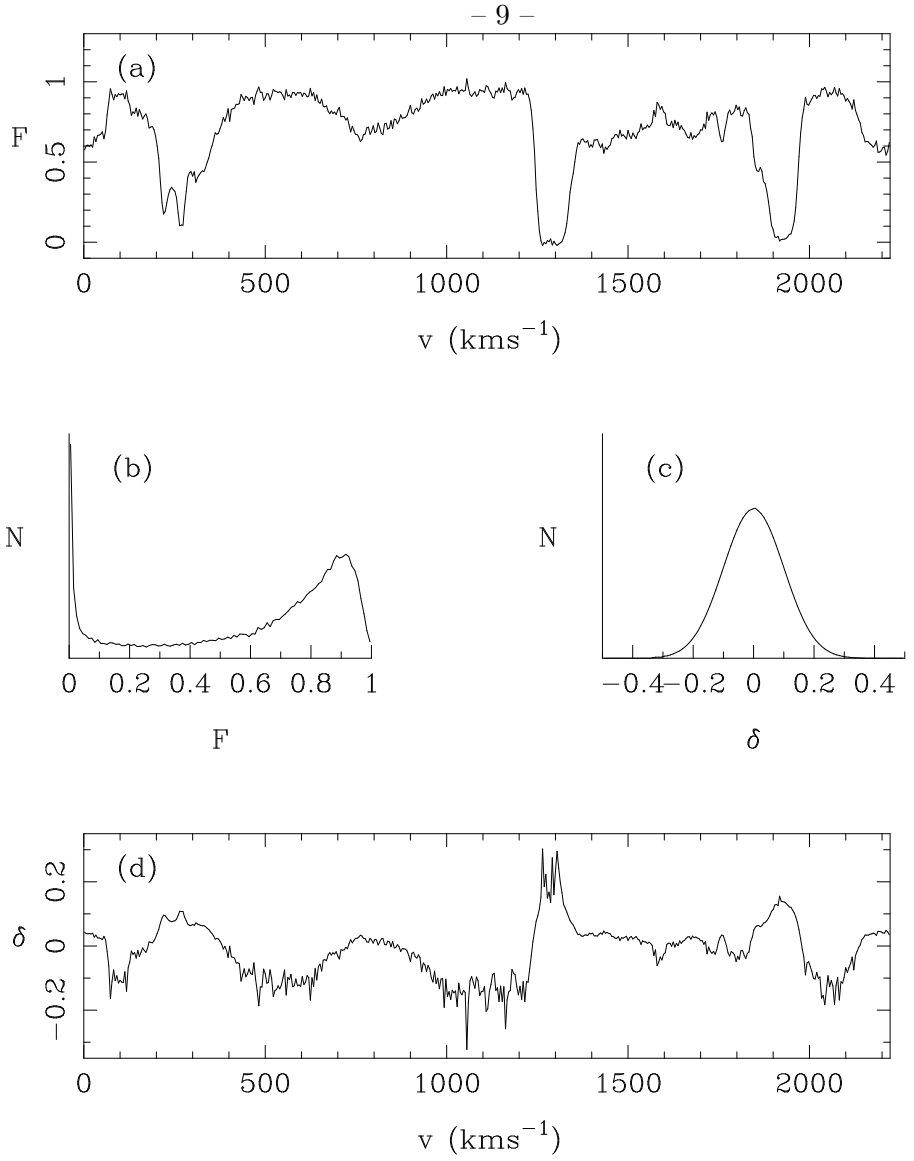

Fig. 1.— Recovery of a line-of-sight initial density field from a QSO Lyα spectrum by Gaussianization. (a) An absorption spectrum taken from a TreeSPH simulation of the SCDM model. Simulated photon noise (S/N=50 in the continuum) has been added. (b) The PDF of pixel flux values in a set of 100 simulated spectra from the same model. (c) The PDF of the inferred initial density contrasts δ. The pixels in the simulated spectra are rank ordered according to their flux values, and each pixel is assigned a density contrast such that the original rank order is retained and $P(\delta)$ is Gaussian. The width of the Gaussian, proportional to the amplitude of the density fluctuations, is arbitrary at this point and will be determined later by the normalization process described in §2.3. (d) The inferred initial density contrast field along the same line of sight as the spectrum in (a).

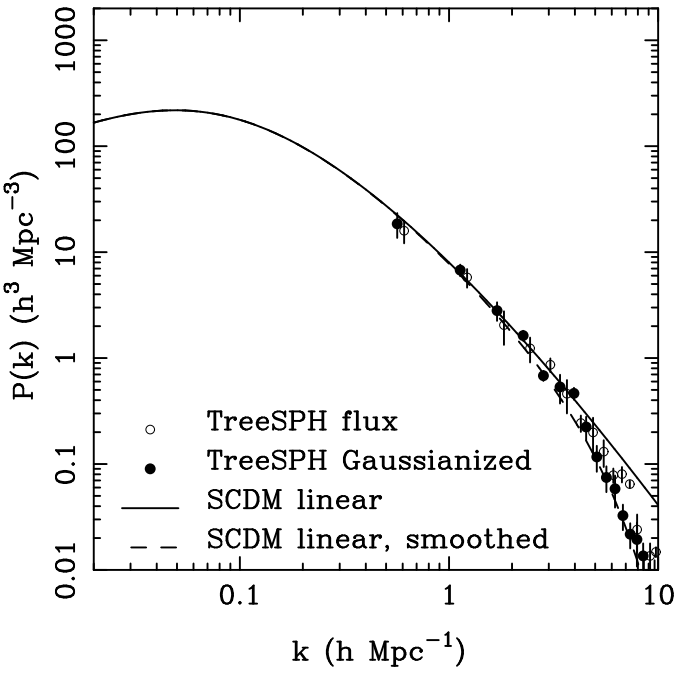

Fig. 2.— Recovery of the power spectrum shape from simulated spectra extracted from the SCDM simulation at $z = 3$, with k in comoving h Mpc^{-1}. Filled circles show $P(k)$ derived from the Gaussianized flux, while open circles show the flux power spectrum itself. Error bars represent the 1σ dispersion among five sets of 20 lines of sight through the simulation, each set roughly equal in redshift path length to an observed QSO spectrum. The derived power spectra are normalized on large scales to match the linear theory SCDM mass power spectrum, shown by the solid line. The dashed line shows the linear theory power spectrum multiplied by $\exp(-\frac{1}{2}k^2r_s^2)$, with $r_s = 1.5\ h^{-1}$Mpc.

error bars on the filled circles in Figure 2 show the 1σ dispersion of these five $P(k)$ estimates and thus indicate the uncertainty in $P(k)$ expected from a single observed QSO spectrum. Note, however, that our 100 spectra are all drawn from the same simulation volume and may therefore underestimate the "cosmic variance" caused by large scale variations in the density field. Also, we have not yet included the effects of instrumental noise and continuum fitting, nor have we indicated the uncertainty in the overall amplitude of $P(k)$ that will arise from our normalization procedure.

On small scales, the recovered $P(k)$ falls below the linear theory power spectrum. The depression of small scale power is caused by the "smearing" of the absorption spectrum by peculiar velocities and thermal broadening and by non-linear gravitational effects that are not fully reversed by Gaussianization. To indicate the scales affected, the dashed line in Figure 2 shows the

linear theory SCDM spectrum multiplied by $\exp(-\frac{1}{2}k^2r_s^2)$ with $r_s = 1.5\ h^{-1}$Mpc. This smoothed linear theory spectrum is a good match to the $P(k)$ derived from the Gaussianized flux. It might be possible to extend the dynamic range of our method by incorporating analytic (or numerical) corrections for this loss of small scale power; however, these corrections might well depend on the assumed cosmological model, and we will not attempt them here.

The power spectrum of the flux also has the same shape as the mass power spectrum on large scales, even though the relation between flux and mass density is highly non-linear. This agreement is reminiscent of Weinberg's (1995) results for locally biased galaxy formation, which show that a non-linear but local relation between galaxy and mass density does not change the shape of the power spectrum on large scales, though it may change the amplitude by a constant factor. The error bars, again derived from the dispersion among five sets of 20 spectra, are slightly larger than those for the Gaussianized flux $P(k)$, probably because Gaussianization "regularizes" the spectra and reduces the impact of rare, strong absorption regions. However, the agreement between the filled and open circles indicates that the recovery of the power spectrum shape is not sensitive to our assumption of a Gaussian primordial PDF — we could recover the shape of $P(k)$ without Gaussianizing at all, at the cost of slightly larger statistical uncertainty. The Gaussian assumption will play a more important role when we normalize $P(k)$ as described in §2.3 below, using simulations with random phase initial conditions.

Figure 3 shows the recovery of the power spectrum shape for the three different cosmological models (SCDM, CCDM, OCDM) for which we have TreeSPH simulations. In each case the normalization is adjusted to match the linear theory $P(k)$ at large scales. Results for the SCDM model are repeated from Figure 2. The power spectrum shape is also correctly recovered for the higher amplitude, CCDM model, though the drop below linear theory shifts to somewhat lower k because of the larger scale of non-linearity. We even recover the subtle difference in shape between the OCDM and SCDM power spectra, though this difference is even smaller when the wavenumber is expressed in directly observable units of $(\text{ km s}^{-1})^{-1}$ (see §4), so a clean distinction will require measurements to larger scales.

Since the three CDM models have similar power spectrum shapes, we want to check that our method can indeed recover the correct shape for a model with a significantly different $P(k)$. Figure 4 shows the $P(k)$ recovered from the Gaussianized flux in a model with an $n = -1$ power law initial power spectrum (and $\Omega = 1$, $h = 0.5$). We do not have a TreeSPH simulation of this model; instead we created artificial spectra by an extended N-body simulation technique described in §2.3 below. At small scales the recovered $P(k)$ is depressed by non-linear evolution and velocity smoothing and is similar to that of the CDM models. However, at $k \lesssim 2.5\ h\ \text{Mpc}^{-1}$ the recovered $P(k)$ bends sharply and matches onto the correct linear theory power spectrum shape, shown by the solid line. Thus, the method is clearly capable of distinguishing an $n = -1$ power law model from a CDM model.

As a further test, we have measured the Gaussianized flux $P(k)$ for a model designed to have

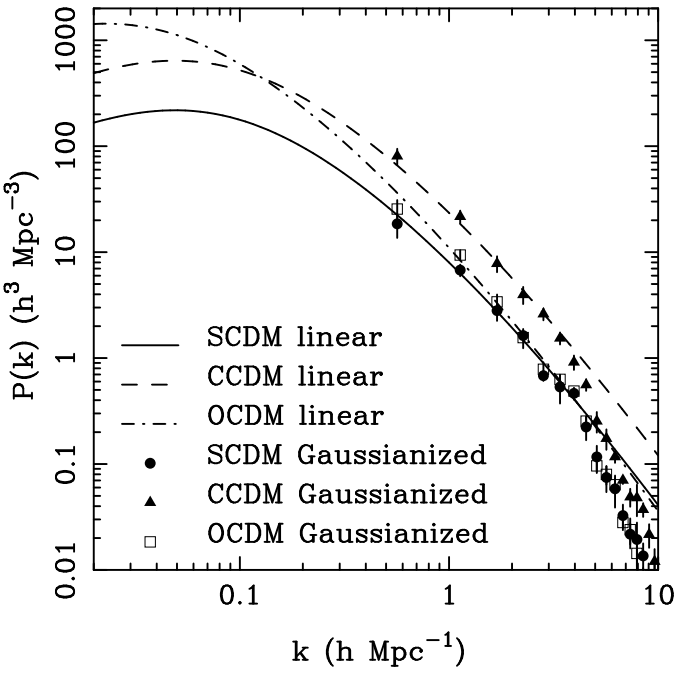

Fig. 3.— Recovery of the power spectrum shape for three different CDM models. Points show $P(k)$ derived from Gaussianized simulated spectra, normalized on large scales to match the corresponding linear theory power spectra shown by the solid (SCDM), dashed (CCDM), and dot-dashed (OCDM) curves. See Fig. 2 caption for further details. In all three cases, the shape of the initial power spectrum is recovered quite accurately for $0.5 \leq k \leq 4\ \ h\ \mathrm{Mpc}^{-1}$.

no large scale clustering. We use a program written by J. Miralda-Escudé that builds up simulated QSO spectra by placing discrete absorption lines with Voigt profiles at random redshifts. The HI column densities of the lines are drawn from a power law distribution $f(n_{\rm HI}) \propto n_{\rm HI}^{-1.5}$ and the b parameters from a truncated Gaussian distribution peaking at $b = 28\ \ \mathrm{km\ s}^{-1}$. The model and parameters are described in more detail in Croft et al. (1997a). The derived power spectrum is shown by the open circles in Figure 4. On small scales we see a "clustering" signal in the Gaussianized flux caused by the finite width of the lines (Zuo & Bond 1994). However, the derived $P(k)$ is consistent with zero for all $k < 2\ h\ \mathrm{Mpc}^{-1}$, as expected given the absence of any intrinsic clustering in the line model. The Gaussianized flux power spectrum can clearly distinguish an unclustered line model from a model where the Lyα forest arises in an intergalactic medium with large scale fluctuations.

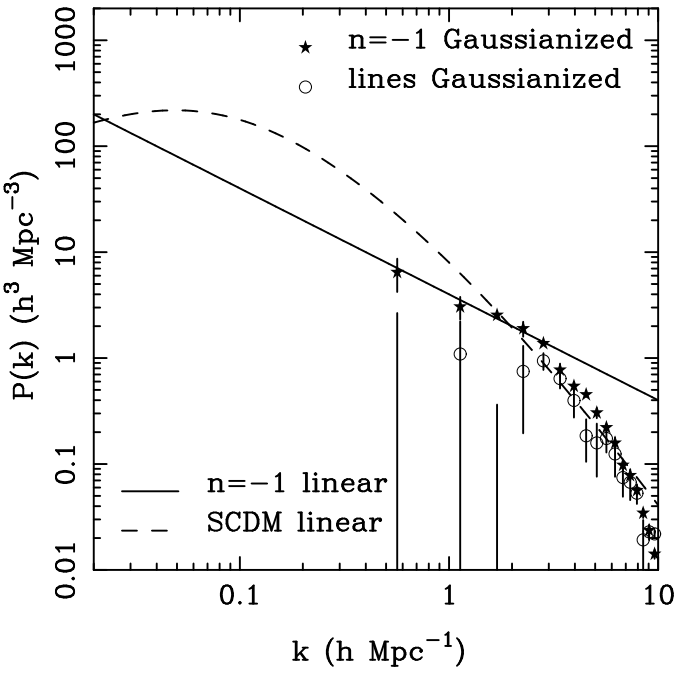

Fig. 4.— The power spectrum of the Gaussianized flux for two non-CDM models. Stars show results for a model with an $n = -1$ power law initial spectrum (the linear theory $P(k)$ is shown as a solid line). Open circles show results from a model where spectra are built from a random superposition of discrete, unclustered lines with Voigt profiles. The linear theory SCDM power spectrum is shown for comparison.

2.3. Power spectrum normalization

Once we have applied the procedure described in §2.2 to simulated or observed QSO spectra, we know the (approximate) shape of the initial power spectrum, but we do not know its amplitude. To determine this normalization, we use the derived $P(k)$ to set up initial conditions for a series of cosmological simulations, with different linear fluctuation amplitudes. We assign random complex phases to the individual Fourier modes, again exploiting the theoretical expectation that the primordial fluctuations are Gaussian. We evolve these simulations to the observed redshift and extract artificial spectra. In simulations with a low fluctuation amplitude, the intergalactic medium (IGM) is relatively smooth, and the extracted spectra show weaker fluctuations than the input spectra. For a high fluctuation amplitude, the simulated IGM is clumpy, and the corresponding Lyα spectra have too much structure. We take the correct linear theory amplitude to be the one for which the extracted Lyα spectra have the correct degree of structure — specifically, we normalize the mass $P(k)$ by requiring that the evolved simulations reproduce the 3-dimensional power spectrum of the (non-Gaussianized) flux on large scales.

This normalization procedure would be computationally impractical if we had to evolve full hydrodynamic simulations for each trial fluctuation amplitude. Fortunately, the physical discussion of the Lyα forest in §2.1 suggests a useful shortcut. We use a particle-mesh (PM) N-body code (Hockney & Eastwood 1981) to evolve a collisionless dark matter simulation from the specified initial conditions. We assume that the baryons trace the dark matter distribution and that the gas temperature is given by the power law temperature–density relation (1). We can then extract Lyα spectra from the simulated gas distribution in the usual fashion and measure their flux power spectra.

This simple, "pseudo-hydro" technique (details given below) is very similar to semi-analytic IGM models that have been used to predict properties of the Lyα forest (Bi 1993; Bi, Ge, & Fang 1995; Reisenegger & Miralda-Escudé 1995; Gnedin & Hui 1996; Bi & Davidsen 1997; Hui, Gnedin, & Zhang 1997), except that these use the lognormal approximation (Coles & Jones 1991) or variations of the Zel'dovich approximation (Zel'dovich 1970) to compute the non-linear dark matter density field. The PM method, being fully non-linear, should yield more accurate results at a still–modest computational cost. A similar numerical approach has been used by Petitjean et al. (1995; see also Mücket et al. 1996) and by Gnedin & Hui (1997; see also Gnedin 1997); both of these groups also incorporate simplified hydrodynamic effects in their PM evolution. We have visually compared spectra computed by the PM approach to spectra produced by TreeSPH from the same initial conditions, and we find good agreement in nearly all regions. The PM technique breaks down in high density regions where shock heating and/or radiative cooling drive gas away from the temperature–density relation (1), which holds only when photoionization heating and adiabatic cooling are the dominant processes affecting the gas temperature. In visual comparisons of our present simulation spectra, we see that these effects appear to be more important than the effects of pressure gradients in limiting the accuracy of the approximation. Our tests below will show that the approximation is adequate for our present purpose, determining the normalization of $P(k)$. Clearly this approximation (or the "hydro-PM" approximation of Gnedin & Hui 1997) is potentially useful for other Lyα forest applications, though its suitability needs to be tested against full hydrodynamic calculations on a case-by-case basis.

In addition to the linear fluctuation amplitude, a number of uncertain parameters must be specified before a given set of initial conditions can be evolved and used to create artificial spectra. These include the cosmological parameters Ω_0, Λ_0, and h, and four parameters that influence the density, temperature, and ionization state of the IGM: Ω_b, T_0, α, and Γ. One might worry that the derived normalization of $P(k)$ would be sensitive to the assumed values of these parameters. Fortunately, the discussion in §2.1 suggests that these parameters collectively influence the Lyα spectrum mainly through a single combination, the constant A in the $\tau - \rho$ relation (2) (the index β has only a slight dependence on these parameters). For a specified initial $P(k)$, the statistical properties of the underlying density field depend mainly on the linear fluctuation amplitude at the redshift in question and are insensitive to cosmological parameters. Once the PM code has provided the density field, the value of A can be determined by matching the observed mean flux

decrement D_A, a constraint that is independent of the flux power spectrum. Our tests below will show that once this mean decrement constraint is imposed the $P(k)$ normalization derived by matching the flux power spectrum is virtually independent of the uncertainties in cosmological and IGM parameters.

Our full procedure for producing spectra from the PM code is as follows:
(a) We generate initial conditions. For the tests in this Section, we want to suppress the statistical fluctuations caused by variations of structure from one simulation to another, and we therefore start our PM simulations from the same initial density fields that were used for the TreeSPH simulations, varying only the linear fluctuation amplitude. In §3 and §4, where we present end-to-end tests of our method and apply it to observations, we generate Gaussian fluctuations with the $P(k)$ shape derived from the input data, using the standard technique of drawing the real and imaginary parts of each Fourier mode from independent Gaussian distributions with mean zero and variance $P(k)/2$. In all cases we use the same box size as the TreeSPH simulations (11.111 h^{-1}Mpc comoving) and 64^3 particles.
(b) We evolve the models from $z = 15$ to $z = 3$ in 20 timesteps (each timestep corresponding to a change in expansion factor $\Delta a = 0.2$). We use a 128^3 mesh for density–potential computations in the PM code. We must adopt values of Ω_0, Λ_0, and h for this evolution, but we will show below that the results are insensitive to this choice.
(c) We interpolate the density and velocity fields onto a 128^3 grid using a cloud-in-cell (CIC) scheme. We then smooth the fields with a Gaussian filter of radius 1 grid cell (following Hui et al. 1997) in order to ensure that velocities are defined everywhere. This scheme is different from the method used to extract line-of-sight fields from the TreeSPH simulations, which involves Lagrangian smoothing with the SPH kernel (see Hernquist et al. 1996). The success of our tests below indicates that the flux power spectrum is insensitive to the detailed procedure used to extract Lyα spectra from a simulation.
(d) We select random lines of sight through the simulation along which to extract spectra. We assign temperatures to each pixel along these lines of sight using the relation $T = T_0\rho^\alpha$. Typical values would be $T_0 \approx 6000$ K, $\alpha = 0.6$, but we will show below that the results do not change for other reasonable choices of T_0 and α.
(e) We adopt provisional values of Ω_b and Γ and compute the neutral hydrogen fraction in each pixel, using its density and temperature and assuming photoionization equilibrium. We compute the Lyα optical depth τ from the neutral hydrogen density.
(f) We map the absorption spectrum $\tau(\lambda)$ from real space to redshift space, redistributing τ values as implied by the peculiar velocity field and convolving with the appropriate thermal broadening.
(g) Finally, we multiply the τ values in all of the spectra by a constant chosen so that the mean flux decrement in the spectra matches the observed D_A. This step is equivalent to changing the parameter combination Ω_b^2/Γ from the provisional value adopted in step (e).

We compute the flux power spectrum as described in §2.2, estimating $P_{\rm 1D}(k)$ by FFT and

deriving the 3-dimensional flux power spectrum, $P_{\rm F}(k)$, using equation (5). The 3-dimensional $P_{\rm F}(k)$ provides a more robust normalization constraint than the 1-dimensional flux power spectrum because we can match power on large scales; $P_{\rm 1D}(k)$ contains aliased small scale power even at low k (eq. [4]). In our flux power spectrum plots we show the quantity $\Delta^2_{\rm F}(k) \equiv k^3 P_{\rm F}(k)$, the contribution of logarithmic k intervals to the variance (Peebles 1980), instead of $P_{\rm F}(k)$. Because the flux power spectra are steep at the scales that we examine, the k^3 factor reduces the dynamic range of the plots and makes it easier to discern differences in amplitude. The use of $\Delta^2_{\rm F}(k)$ also minimizes potential confusion with our plots of the recovered mass fluctuation power spectrum, where we will continue to show $P(k)$ itself. We note here that the flux power spectrum, $\Delta^2_{\rm F}(k)$, is an interesting statistic in its own right, and can be used as a measure of structure in the Lyα forest. However, in this paper we will concern ourselves solely with its usefulness in determining the normalization of the mass power spectrum $P(k)$.

Figure 5 demonstrates the sensitivity of $\Delta^2_{\rm F}(k)$ to the amplitude of linear theory mass fluctuations. The points show $\Delta^2_{\rm F}(k)$ measured from the three TreeSPH simulations, with error bars calculated as in the previous figures from the 1σ dispersion among five sets of 20 spectra each. The lines show $\Delta^2_{\rm F}(k)$ computed from PM simulations that have the same initial fluctuations as the corresponding TreeSPH simulations but different linear theory amplitudes. We evolve the PM simulations using the appropriate cosmological parameters (Ω_0, Λ_0, and h) and extract spectra as described above, using the temperature–density relation measured from the corresponding TreeSPH run (e.g., $T_0 = 5600$ K, $\alpha = 0.6$ for SCDM). We label each curve by σ_8, the rms linear theory mass fluctuation in 8 h^{-1}Mpc spheres at $z = 0$ implied by the adopted power spectrum normalization. Figure 5 shows results at $z = 3$, when the linear theory amplitudes are lower by a factor of 4.0 in the two $\Omega = 1$ models and 2.71 in the open model. We measure $\Delta^2_{\rm F}(k)$ from 1000 lines of sight for each PM simulation, enough that the fluctuations in the $\Delta^2_{\rm F}(k)$ curves do not change with the addition of more spectra. Some fluctuations remain because we are always simulating a single 11.111 h^{-1}Mpc box with the same initial phases and therefore have a finite number of independent structures in the evolved gas distribution. We use the same initial phases for the PM and TreeSPH runs in this Section in order to limit the effect of this cosmic variance on the $\Delta^2_{\rm F}(k)$ comparisons.

As expected, on large scales ($k \lesssim 2\ h\ {\rm Mpc}^{-1}$) the amplitude of the flux power spectrum increases steadily with increasing mass fluctuation amplitude. On small scales the $\Delta^2_{\rm F}(k)$ curves turn over because of non-linear gravitational evolution and blurring of the Lyα spectra by peculiar velocities, and the curves for $\sigma_8 > 0.4$ converge. In each panel of Figure 5, we use a heavy solid line to indicate the $\Delta^2_{\rm F}(k)$ curve from the PM simulation with the correct linear theory amplitude. In all cases, this curve provides the best overall visual fit to the $\Delta^2_{\rm F}(k)$ values obtained from the TreeSPH simulation. Figure 5 thus demonstrates two essential points: the flux power spectrum at small k is sensitive to the mass fluctuation amplitude, making it an appropriate fitting constraint for $P(k)$ normalization, and the PM approximation is accurate enough for determining this normalization properly.

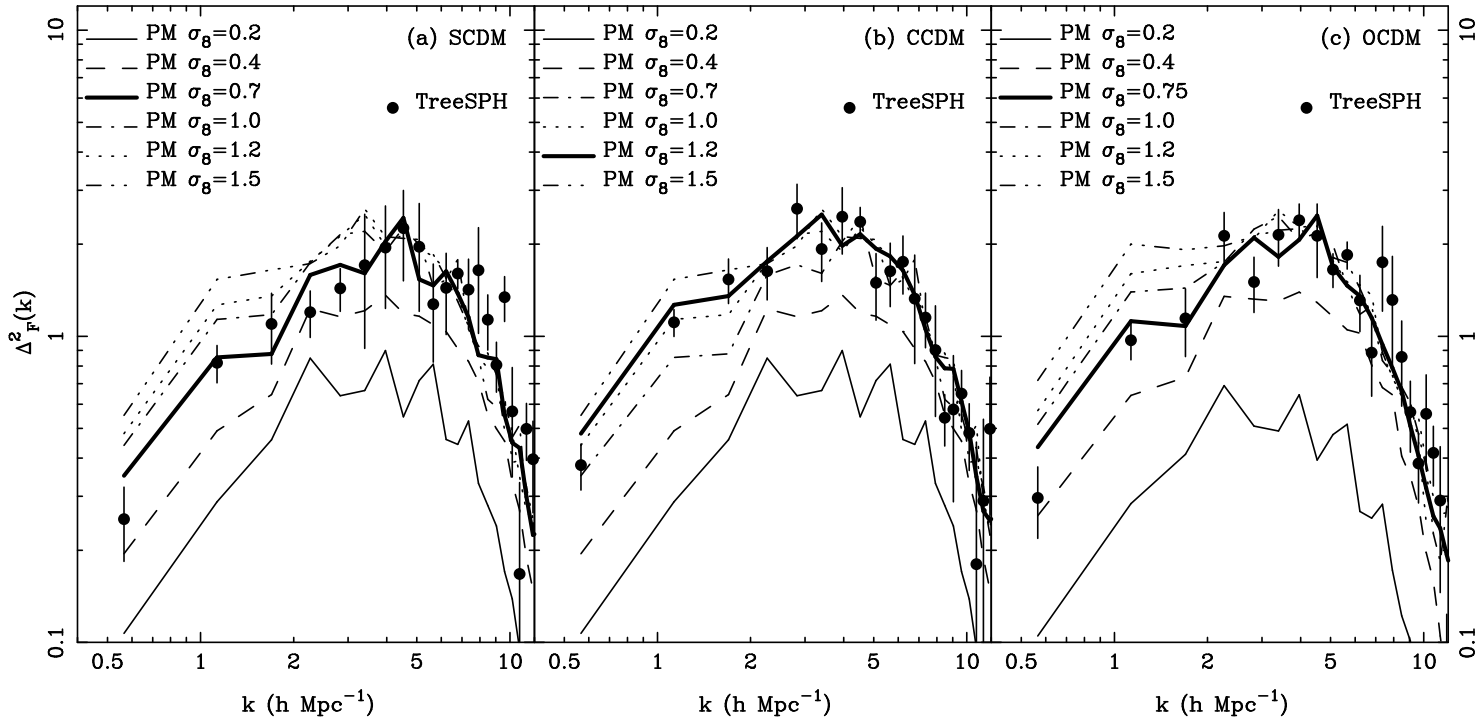

Fig. 5.— Dependence of the flux power spectrum $\Delta^2_{\rm F}(k)$ on the amplitude of underlying mass fluctuations. Results are shown at $z = 3$ for the (a) SCDM, (b) CCDM, and (c) OCDM models. In each panel, points show $\Delta^2_{\rm F}(k)$ for 100 spectra from the TreeSPH simulation, with error bars computed from the 1σ scatter among five groups of 20 spectra each. Lines show $\Delta^2_{\rm F}(k)$ from 1000 spectra extracted from PM simulations with the same initial fluctuations as the TreeSPH simulation but different linear theory amplitudes, which are indicated in the legends. In each case, the heavy solid line shows the PM results for the linear theory amplitude used in the corresponding TreeSPH simulation.

As mentioned above, we choose the value of Ω_b^2/Γ for each PM fluctuation amplitude to match the mean flux decrement of the TreeSPH spectra, $D_A(z = 3) = 0.36$. As the mass fluctuation amplitude increases, more of the gas flows into near-saturated regions, and a higher value of Ω_b^2/Γ is required to give the correct D_A. For example, the PM simulations of SCDM require a value of Ω_b^2/Γ 2.4 times higher for $\sigma_8 = 1.2$ than for $\sigma_8 = 0.7$, consistent with the results from the TreeSPH simulations themselves (see Croft et al. 1997a).

Figure 6 highlights the importance of the mean flux decrement constraint to the normalization procedure. The points and heavy solid line, repeated from Figure 5a, show, respectively, $\Delta^2_{\rm F}(k)$ from the TreeSPH simulation and from the PM simulation with the correct linear theory amplitude and a value of Ω_b^2/Γ that yields $D_A = 0.36$. The dashed line and thin solid line show $\Delta^2_{\rm F}(k)$ from the same PM simulation with the value of Ω_b^2/Γ respectively increased and decreased by a

factor of two. These changes alter $\Delta^2_{\rm F}(k)$ by about a factor of two at large scales, roughly what one might expect from the physical discussion in §2.1. The changes to Ω_b^2/Γ alter the constant A in the $\tau - \rho$ relation (2) by a factor of two, and this constant serves as a sort of "bias factor" between density fluctuations and optical depth fluctuations. In studies of galaxy clustering, the bias between galaxies and mass is not known a priori; if it is assumed to be independent of scale, then one obtains the shape of the mass power spectrum but not its amplitude. We can obtain the shape *and amplitude* of the mass power spectrum from Lyα forest observations because the mean flux decrement provides an observational constraint on the effective "bias factor" that is independent of the flux power spectrum itself — D_A measures the mean Lyα opacity, while $\Delta^2_{\rm F}(k)$ measures fluctuations about the mean. High precision estimates of the amplitude of mass fluctuations require reliable measurements of D_A from observations. Current estimates of D_A are not all consistent (e.g., compare Press et al. 1993 and Rauch et al. 1997 with Zuo & Lu 1993), a situation that must be resolved in order to make the most of our normalization procedure.

From equation (2), it is clear that the value of Ω_b^2/Γ needed to match D_A for a given density field will itself depend on the adopted values of the IGM parameters T_0 and α and the cosmological parameters Ω_0, Λ_0, and h, which collectively determine $H(z)$. To the extent that the approximation (2) holds, the effects of changing these parameters and of changing Ω_b^2/Γ are degenerate (except for the small influence of α on the index of the $\tau - \rho$ relation). Normalizing to the observed D_A therefore eliminates their influence on the derived amplitude of mass fluctuations. However, varying these parameters also changes the amount of thermal broadening and peculiar velocity distortion in the Lyα spectrum (eq. [2] ignores these effects), and we must check that such variations do not thereby alter the inferred $P(k)$ normalization.

Figure 7 illustrates the effects of T_0 and α on $\Delta^2_{\rm F}(k)$ at fixed D_A. The filled circles and heavy solid line, repeated from Figures 5a and 6, show $\Delta^2_{\rm F}(k)$ obtained, respectively, from the SCDM TreeSPH simulation and from the PM simulation with the same initial conditions and the values $T_0 = 5600$ K, $\alpha = 0.6$ that fit the temperature–density relation of the TreeSPH run. The other lines show $\Delta^2_{\rm F}(k)$ obtained from the PM simulation with different (rather extreme) values of T_0 and α. For each combination of T_0 and α, we adjust Ω_b^2/Γ so that the mean flux decrement of the PM spectra is $D_A = 0.36$; for example, Ω_b^2/Γ is 2.2 times higher for $T_0 = 20,000$ K than for $T_0 = 5600$ K. With the D_A constraint imposed, we see that $\Delta^2_{\rm F}(k)$ is almost completely insensitive to the value of α and to a factor ~ 4 increase or decrease in T_0. For $T_0 = 20,000$ K, the larger degree of thermal broadening depresses $\Delta^2_{\rm F}(k)$ on small scales, but even this extreme variation does not significantly alter $\Delta^2_{\rm F}(k)$ for $k \lesssim 2\ h\ {\rm Mpc}^{-1}$.

Changes in the cosmic reionization history and the spectral shape of the UV background influence the low density IGM through the parameters T_0 and α (Hui & Gnedin 1997). Since Figure 7 shows that changing T_0 and α does not alter $\Delta^2_{\rm F}(k)$ if D_A is held fixed, we conclude that uncertainties in the reionization history and UV background spectral shape do not affect our ability to normalize $P(k)$ accurately.

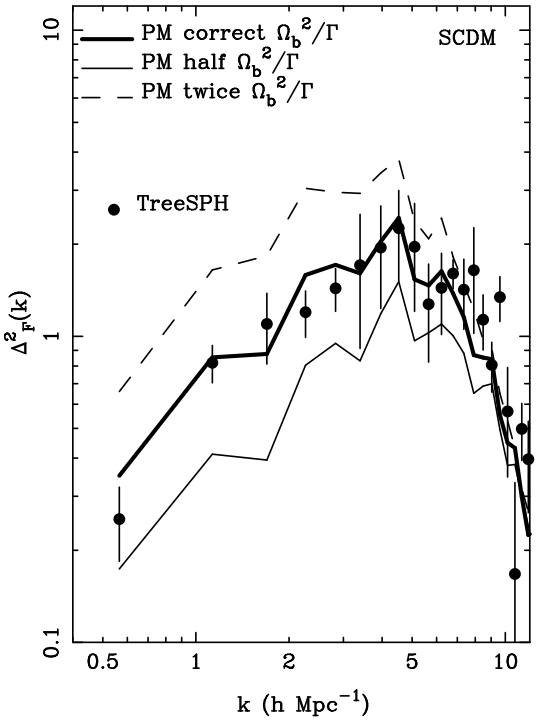

Fig. 6.— Dependence of $\Delta^2_{\rm F}(k)$ on the value of Ω_b^2/Γ. Filled circles (repeated from Fig. 5a) show $\Delta^2_{\rm F}(k)$ from the SCDM TreeSPH simulation. The heavy solid line (also repeated from Fig. 5a) shows $\Delta^2_{\rm F}(k)$ from the PM simulation with the correct mass fluctuation amplitude and Ω_b^2/Γ chosen to reproduce the mean flux decrement of the TreeSPH spectra, $D_A = 0.36$. The other lines show $\Delta^2_{\rm F}(k)$ from the same PM simulation with Ω_b^2/Γ increased (dashed line) and decreased (thin solid line) by a factor of two, corresponding to lower and higher values of D_A, respectively. These results demonstrate the importance of fixing Ω_b^2/Γ to yield the observed D_A when normalizing the mass power spectrum on large scales.

Figure 8 shows the influence of changing the cosmological parameters Ω_0, Λ_0, and h on $\Delta^2_{\rm F}(k)$. The filled circles in panels (a) and (b) show the TreeSPH results for the SCDM and OCDM models, respectively, as in Figures 5a and 5c. In each panel the heavy solid line (again repeated from the corresponding panel of Figure 5) shows $\Delta^2_{\rm F}(k)$ from the PM simulation with the correct mass fluctuation amplitude, temperature–density relation, and cosmological parameters. The other lines show results from PM simulations with the same linear theory density fluctuations and temperature–density relation but different values of the cosmological parameters. In each PM simulation we adopt a comoving box size of 11.111 h^{-1}Mpc and scale the amplitude of the initial fluctuations (at $z = 15$) so that their linear theory amplitude at $z = 3$ matches that of the corresponding TreeSPH simulation. We also adjust Ω_b^2/Γ to keep $D_A = 0.36$.

With D_A and the linear theory mass fluctuations held fixed, $\Delta^2_{\rm F}(k)$ is insensitive to the

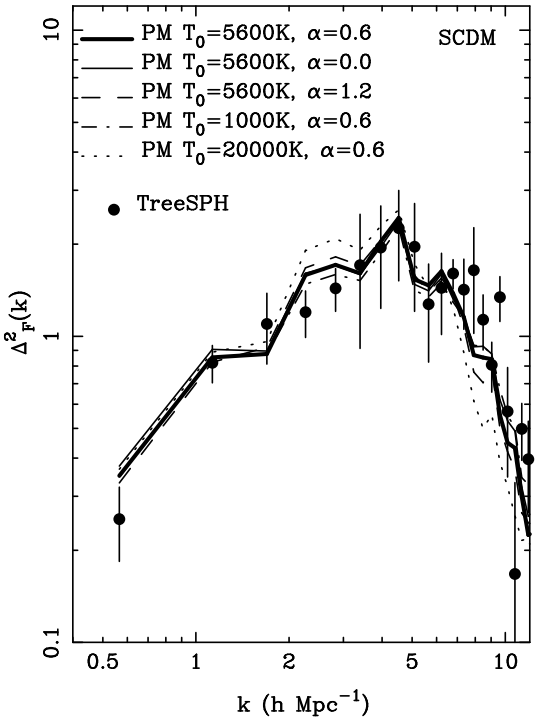

Fig. 7.— Dependence of $\Delta^2_{\rm F}(k)$ on the IGM parameters T_0 and α. The filled circles and the heavy solid line, repeated from Fig. 5a, show $\Delta^2_{\rm F}(k)$ from the SCDM TreeSPH simulation and from the PM simulation with the same initial conditions and temperature-density relation. Other lines show $\Delta^2_{\rm F}(k)$ from the PM simulation with different values of T_0 and α. In each case, Ω_b^2/Γ is chosen to keep the mean flux decrement $D_A = 0.36$. With this constraint imposed, $\Delta^2_{\rm F}(k)$ is insensitive to the adopted values of T_0 and α.

adopted cosmological parameters. Except in the cores of virialized objects, the non-linear mass density field depends almost exclusively on the linear theory mass fluctuations, independent of Ω_0 and Λ_0 (Weinberg & Gunn 1990; Nusser & Colberg 1997). Linear theory peculiar velocities are approximately proportional to $\Omega^{0.6}$ (Peebles 1980), but at high redshift Ω is always close to one; for $\Omega_0 = 0.4$, the $\Omega^{0.6}$ factor at $z = 3$ is 0.83 in the open model and 0.99 in the flat, non-zero Λ model. The value of $H(z)$ depends on Ω_0, Λ_0, and h, but the overall scaling of optical depths with $H^{-1}(z)$ is removed by the D_A normalization. For fixed T_0 and α, the importance of thermal motions relative to Hubble flow and peculiar velocities is larger when $H(z)$ is smaller, but even for small $H(z)$ the impact of thermal broadening on $\Delta^2_{\rm F}(k)$ is insignificant. Other statistical properties of the flux might be able to detect the direct influence of these cosmological parameters, but our normalization of $P(k)$ will not depend on them. Note, however, that once other observational constraints are imposed (for example, the abundance of massive galaxy clusters at $z = 0$, or the amplitude of CMB anisotropies), the $P(k)$ predicted on Mpc scales at high redshift will depend on the adopted cosmological parameters. Thus, the combination of $P(k)$ from QSO spectra with

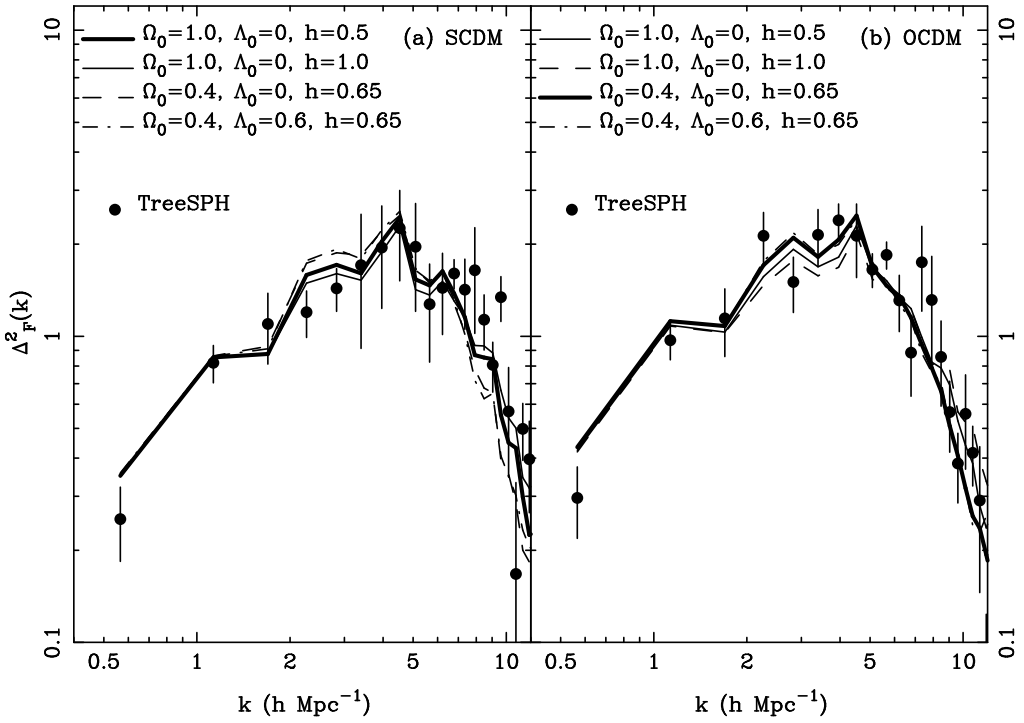

Fig. 8.— Dependence of $\Delta^2_{\rm F}(k)$ on cosmological parameters, with D_A and the linear theory mass fluctuations at $z = 3$ held fixed. Filled circles show $\Delta^2_{\rm F}(k)$ from TreeSPH simulations of (a) the SCDM model and (b) the OCDM model, as in Figs. 5a and 5c. Bold solid lines (also repeated from Fig. 5) show $\Delta^2_{\rm F}(k)$ from PM simulations with the same cosmological parameters. Other lines show results from PM simulations evolved with different cosmological parameters, indicated in the legends. In each case, the amplitude of fluctuations at the start of the simulation ($z = 15$) is chosen so that the linear theory amplitude at $z = 3$ is the same as that for the corresponding TreeSPH simulation.

other robust observational measures can provide critical tests of cosmological models. We will return to this issue in §5.

In our tests so far, we have evolved PM simulations from the same initial fluctuations as the TreeSPH simulations, varying only the amplitude. However, Figure 2 shows that the mass power spectrum inferred from the Gaussianized Lyα flux is systematically depressed on small scales, and we must check that this systematic error in the *shape* of $P(k)$ at high k does not change the *amplitude* of $P(k)$ inferred by matching $\Delta^2_{\rm F}(k)$ at lower k. As shown in Figure 2, the small scale depression is roughly equivalent to smoothing the true $P(k)$ with a Gaussian filter of comoving radius 1.5 h^{-1}Mpc. Figure 9 shows the flux power spectrum $\Delta^2_{\rm F}(k)$ from the TreeSPH, SCDM simulation and from the PM simulation evolved from the same initial conditions, as in Figure 5a. The thin solid line shows $\Delta^2_{\rm F}(k)$ from a PM simulation in which the initial fluctuations are

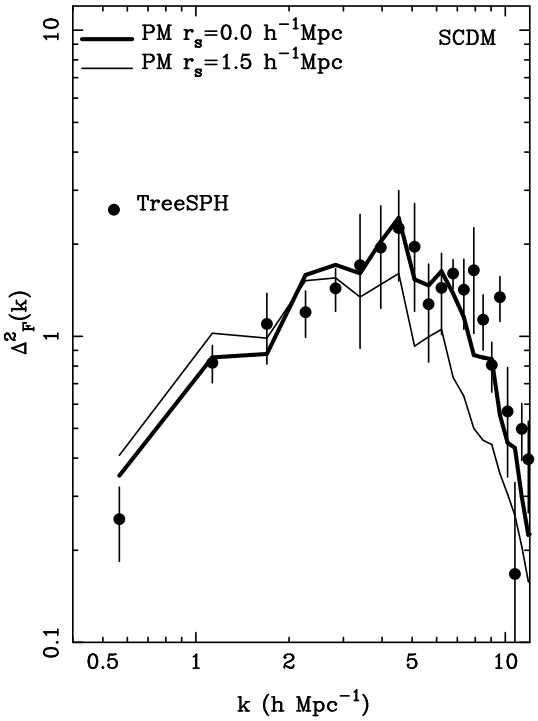

Fig. 9.— Dependence of $\Delta^2_{\rm F}(k)$ on small scale power in the initial fluctuations. Filled circles and the heavy solid line show $\Delta^2_{\rm F}(k)$ from the TreeSPH and PM simulations of the SCDM model, as in Fig. 5a. The thin solid line shows $\Delta^2_{\rm F}(k)$ from a PM simulation evolved from the same initial conditions smoothed with a 1.5 h^{-1}Mpc Gaussian filter, to approximate the loss of small scale power seen in Fig. 2.

smoothed with a 1.5 h^{-1}Mpc Gaussian filter before they are evolved forward. As one might expect, $\Delta^2_{\rm F}(k)$ at $z = 3$ is somewhat lower at high k because of the reduced small scale power in the initial fluctuations. However, on the larger scales that we use for determining the $P(k)$ normalization, the smoothing of the initial conditions has little effect. One could slightly improve the accuracy of the normalization procedure by amplifying the small scale power in the Gaussianized flux $P(k)$ before the PM evolution step, but to keep the presentation of our method reasonably simple, we will not include such corrections in this paper.

The results of this Section are encouraging and easy to summarize. The flux power spectrum $\Delta^2_{\rm F}(k)$ depends directly on the linear theory amplitude of mass fluctuations, and it is insensitive to the adopted values of IGM parameters and cosmological parameters as long as one adjusts Ω_b^2/Γ to match the mean flux decrement D_A to the observed value. The PM approximation provides an accurate and inexpensive method to compute $\Delta^2_{\rm F}(k)$. We therefore have a practical and robust procedure for determining the normalization of $P(k)$, once its shape has been derived from the Gaussianized Lyα flux as described in §2.2.

2.4. Effects of noise, resolution, and continuum fitting

Real QSO spectra may have coarser resolution than our simulated spectra, and they are affected by photon noise from the QSO and the sky and by instrumental readout noise. The throughput of the atmosphere and instrument as a function of wavelength may not be known exactly, and in any case one does not have precise a priori knowledge of the underlying QSO continuum in the Lyα forest region. Therefore, the flux level corresponding to zero absorption is usually determined from the spectrum itself by a local continuum fitting procedure. In this Section, we will add noise to the TreeSPH spectra, degrade their spectral resolution, and apply local continuum fitting to see how these observational realities affect our ability to determine $P(k)$.

To model the effect of limited spectral resolution, we take the simple approach of rebinning the TreeSPH spectra (which have ~ 2 km s^{-1} pixels) into larger pixels — a "top hat" smoothing of the transmitted flux. We then add photon noise with a specified signal-to-noise ratio S/N in the continuum. For each pixel, we draw the photon noise from a Poisson distribution with a mean proportional to the transmitted flux level, effectively assuming the limit where noise from the QSO itself dominates over noise from the sky. A more thorough treatment of sky photon noise requires specifying the QSO and sky flux at the observed Lyα forest wavelengths; we defer detailed tests of these effects to a later paper where we analyze a large observational data set. In addition to photon noise, we add noise drawn from a Gaussian distribution with zero mean and standard deviation $\Delta F = 0.01$ (where $F = 1$ represents the unabsorbed continuum), independent of the pixel flux level, to model instrument readout noise.

We try three different combinations of spectral resolution/noise parameters:
(1) High resolution (4 km s^{-1} pixels), high S/N (50 per resolution element in the continuum). These values are characteristic of a typical Keck HIRES spectrum (e.g., Hu et al. 1995).
(2) High resolution (4 km s^{-1} pixels), low S/N (10 per resolution element).
(3) Low resolution (40 km s^{-1} pixels), low S/N (10 per resolution element).
Since we degrade the spectral resolution by top hat rebinning, a "resolution element" is simply a pixel of the rebinned spectrum.

The implicit assumptions in standard continuum fitting procedures are that the QSO continuum and instrumental response vary slowly as a function of wavelength and that the highest observed flux levels correspond to the unabsorbed continuum (plus noise). In high resolution, echelle spectra, the continuum is often determined separately for each echelle order by (1) fitting a 3rd-order polynomial to the data points, (2) rejecting all points that lie more than 2-σ below this polynomial fit, and (3) repeating the process with the points that remain, iterating until the continuum fit converges. This is the procedure that we will use here (it was also used by Davé et al. 1997). Each of our simulated spectra is periodic on the scale of the simulation box, which at $z = 3$ corresponds to $36\mathring{A}$ in the SCDM and CCDM simulations and $27\mathring{A}$ in the OCDM simulation. This scale is shorter than the $\sim 45\mathring{A}$ length of a typical Keck HIRES echelle order. In order to partially account for this difference in length and reduce edge effects, we periodically extend each

spectrum by an equal length on either side of the simulation box to create a 45$\AA$ region. We fit the continuum to this region. Nonetheless, the systematic depression of the continuum below its true value should be larger in our simulated observations than in real data because there is less chance of finding a region of genuinely low absorption in the short spectra we have available. Our tests should therefore give an upper limit to the effects of continuum fitting on the determination of $P(k)$.

Figure 10 illustrates the effect of continuum fitting on several example spectra from the SCDM simulation, for the high resolution, high S/N and low resolution, low S/N observational parameters. In each panel, the heavy solid line shows the TreeSPH spectrum, rebinned to the appropriate spectral resolution, with added noise. The dotted line shows the fitted continuum. Light solid lines show the renormalized spectra, with the original flux in each pixel divided by the local continuum level. Clearly the main effect of continuum fitting and renormalization is to remove absorption (boost the flux) in low density regions, since the fitted continuum is systematically depressed there. The effect is largest for the low resolution, low S/N spectra, where the mean flux decrement is reduced by $\sim 14\%$. In the high resolution, high S/N spectra, continuum renormalization reduces the mean flux decrement by $\sim 5\%$.

Figure 11 shows how noise and continuum fitting influence the shape of $P(k)$ derived from the Gaussianized flux. These results from the degraded spectra can be compared to those from the noiseless spectra shown in Figure 2. The low resolution, low S/N spectra give somewhat noisier $P(k)$ estimates at small scales, but noise and continuum fitting do not appear to distort the shape of the inferred $P(k)$. The largest scale points ($2\pi/k = 11.111\ h^{-1}$Mpc) lie a factor ~ 2 below the linear theory power spectrum. Since there are only a few modes at this scale in our simulation box, this depression of large scale power could be a statistical fluctuation, but it could also be a systematic effect of continuum fitting, which tends to even out large scale fluctuations. The uncertainties in continuum determination may ultimately set the upper limit to the scale where $P(k)$ can be determined reliably from the Lyα forest. This question is best addressed in the context of specific observational data using larger volume simulations, and we therefore defer a more thorough investigation of continuum fitting procedures and their effects to future work. For now, we note that Figure 11 shows that there is an interesting range of scales over which noise and continuum fitting do not pose serious problems for the determination of the shape of $P(k)$.

Noise and continuum fitting have even less impact on the normalization of $P(k)$ using $\Delta^2_{\rm F}(k)$. Figure 12 shows $\Delta^2_{\rm F}(k)$ in the SCDM model measured from the noiseless TreeSPH spectra (points with error bars, repeated from Figure 5a) and from the degraded, continuum–renormalized spectra. The flux power spectrum cuts off on small scales in the low resolution spectra as one might expect, but $\Delta^2_{\rm F}(k)$ is virtually unchanged on the larger scales that we use for normalization. Even with 40 km s^{-1} pixels the suppression of power is limited to scales a factor of two smaller than those where the Gaussianized flux power spectrum matches the linear theory mass $P(k)$ (see Figure 11), suggesting that we could use still coarser resolution spectra for power spectrum determination without losing useful information. (However, continuum determination might be more problematic

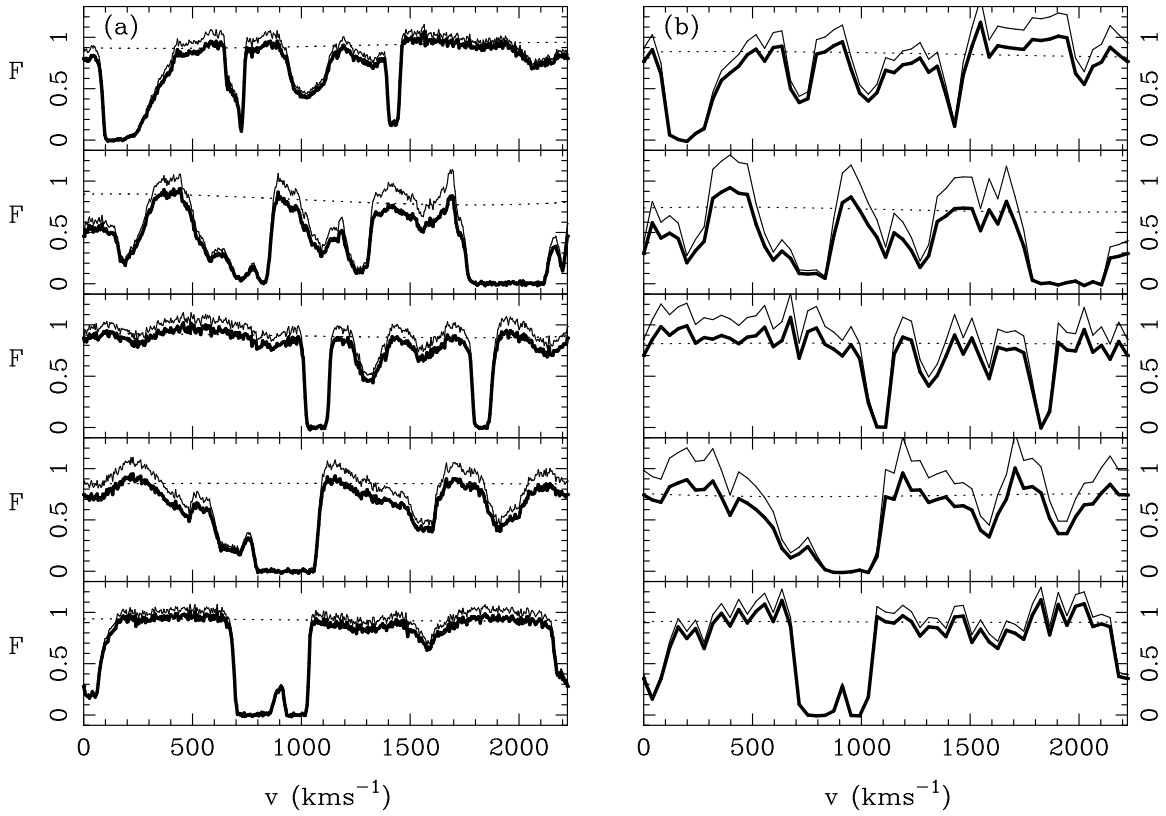

Fig. 10.— The effects of continuum fitting and renormalization on simulated spectra from the SCDM model at $z = 3$, for (a) 4 km s^{-1} pixels and S/N=50, (b) 40 km s^{-1} pixels and S/N=10. In each panel, the heavy solid lines shows the simulated spectrum with degraded spectral resolution and added noise. The dotted line shows the continuum estimated by the 3rd-order polynomial fitting procedure described in the text. The thin solid line shows the renormalized spectrum, with the original flux in each pixel divided by the fitted continuum level.

in lower resolution spectra, so we might ultimately lose information on *large* scales.) In general, pixel–scale variations in detector response (e.g., flat–fielding errors, cosmic rays) only affect $\Delta^2_{\rm F}(k)$ and $P(k)$ at high k, where our recovery is limited in any case by the effects of peculiar velocities, thermal motions, and non-linear evolution. It is only large scale, coherent variations that are cause for concern. As Figure 5 shows, the fluctuation amplitudes (per logarithmic k bin) predicted by CDM models are of order unity on the scales considered in this paper, so any systematic errors would have to be quite substantial to influence the recovered power spectrum.

3. A test of the entire procedure on simulated observations

We have now tested all of the pieces of our power spectrum recovery method individually. For the tests in §2, we have always used the same initial density field that was used in the

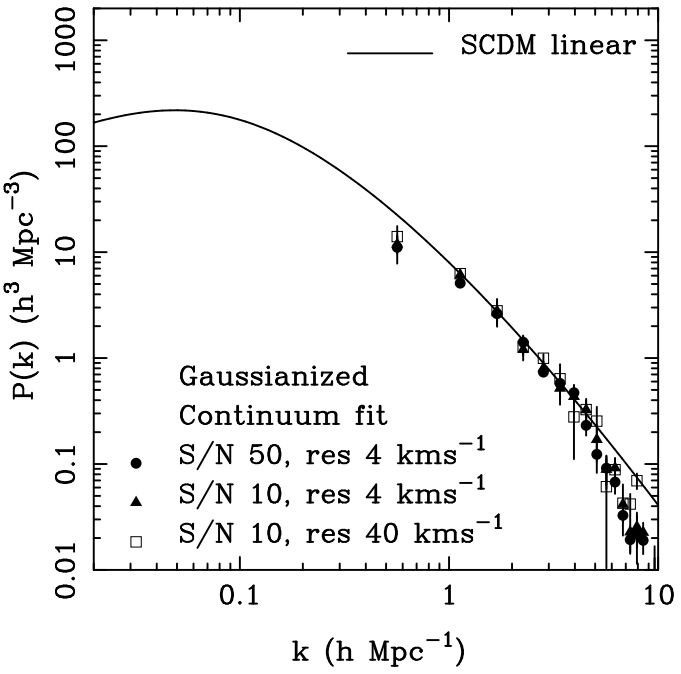

Fig. 11.— The effects of noise, spectral resolution, and continuum fitting on the shape of the power spectrum derived from the Gaussianized flux. Points show $P(k)$ estimated from the continuum-renormalized, degraded TreeSPH spectra, with the observational parameters indicated in the legend. Error bars show the 1σ dispersion among five sets of 20 spectra each. Amplitudes of the derived $P(k)$ are chosen to match the SCDM linear theory power spectrum, shown by the solid line. These results can be compared to those from noiseless spectra, shown in Fig. 2.

TreeSPH simulations, in order to separate errors in the recovery procedure from the statistical fluctuations in finite–volume realizations of a given model. In this Section we will treat spectra from the TreeSPH simulations as if they were observational data, and attempt to recover the mass power spectrum from them without using prior knowledge of the initial conditions or cosmological parameters. Comparison of the results to the models' true linear power spectra will provide end–to–end tests of the full $P(k)$ recovery procedure.

As our starting point, we take the low resolution, low S/N spectra from §2.4. These are the worst case observational parameters that we have considered, and if the procedure works well for these spectra then it should be very widely applicable in practice. We generate 100 spectra for each of the three cosmological models, fitting a continuum to each spectrum as described in §2.4. We will again compute error bars from the dispersion among five sets of 20 spectra, each set roughly equal in redshift path length to a single observed QSO spectrum. One caveat to bear in mind is that these five simulated "QSOs" probe the structure in a single simulation box; on

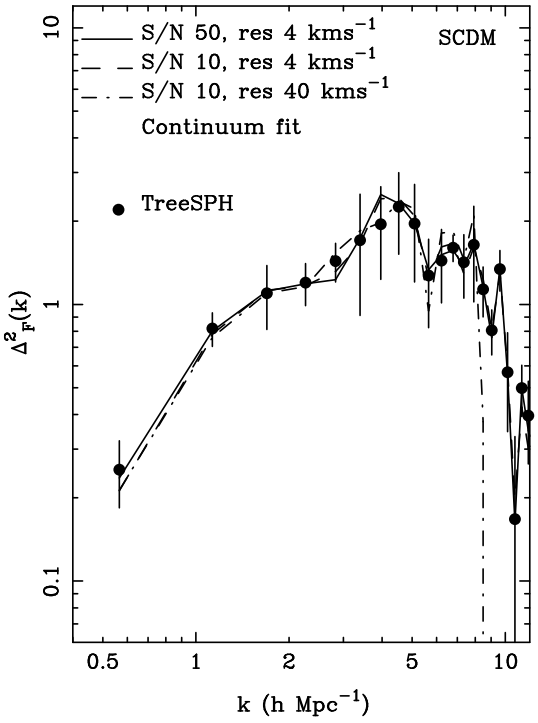

Fig. 12.— The effects of noise, spectral resolution, and continuum fitting on the flux power spectrum. Points with error bars (repeated from Fig. 5a) show $\Delta^2_{\rm F}(k)$ from noiseless, TreeSPH, SCDM spectra. Lines show $\Delta^2_{\rm F}(k)$ measured from continuum–renormalized spectra with the noise and resolution parameters indicated in the legend.

scales comparable to the box, there are only a handful of Fourier modes, and their average power may not equal the true cosmic average predicted by the model. Real spectra of the same total path length would sample more independent large scale fluctuations and should therefore yield an average $P(k)$ closer to the true value. However, the dispersion in $P(k)$ estimates from one spectrum to another should also be larger if they are fully independent, so the statistical error bars that we derive will be somewhat underestimated.

To recap, the steps of the $P(k)$ recovery procedure are as follows:
(1) Gaussianization. We reassign pixel flux values so that they have a Gaussian PDF but the same rank order as in the original spectrum. This step yields an unnormalized estimate of the linear density contrast field along each line of sight.
(2) Measurement of the shape of $P(k)$. We estimate the 1-dimensional power spectrum of the Gaussianized flux using an FFT. We convert to the 3-dimensional $P(k)$ using equation (5).
(3) Determination of the amplitude of $P(k)$.
(a) We use $P(k)$ from step (2) to create realizations of an initial, random phase, linear density field. We evolve each density field forward under gravity using a PM code. We choose the

cosmological parameters relevant to the SCDM model ($\Omega_0 = 1$, $\Lambda_0 = 0$, $h = 0.5$) to do this, but we have seen in §2.3 that any other choice will make essentially no difference to the results.
(b) At each of several output times, we generate spectra using a power law temperature–density relation (any reasonable choice of T_0 and α in eq. [1] will do) and the value of Ω_b^2/Γ that yields the same mean flux decrement as the input spectra, in this case $D_A = 0.36$. Because the linear density contrast grows in proportion to the expansion factor in an $\Omega = 1$ universe, the multiple output times of a single simulation are physically equivalent to the outputs at a fixed time (or redshift) of simulations with different amplitudes of the linear theory mass power spectrum.
(c) We estimate $\Delta_{\rm F}^2(k)$ for each mass fluctuation amplitude, averaging results obtained from several realizations of the initial density field that have the same $P(k)$ but different random phases. We compare these $\Delta_{\rm F}^2(k)$ values to those measured from the "observed" spectra, on large scales. The normalization of $P(k)$ is found by linearly interpolating between the output times (fluctuation amplitudes) that reproduce the $\Delta_{\rm F}^2(k)$ amplitude most closely.

We apply this procedure to the three CDM models in turn. For the normalization step, we use four different random phase realizations in each case, with PM simulation boxes 11.111 h^{-1}Mpc on a side, matched to the TreeSPH simulations. We extract spectra along 1000 lines of sight from each simulation cube at each output. Figure 13 shows the $\Delta_{\rm F}^2(k)$ results used in the normalization step for the three models. For the wavenumber k, we now use (km s^{-1})$^{-1}$ units, since these can be related directly to observed wavelength. The conversion from km s^{-1} to comoving h^{-1}Mpc would depend on our adopted cosmological parameters. At $z = 3$, the SCDM and CCDM simulation cubes are 2222 km s^{-1} on a side, but the OCDM simulation is 1647 km s^{-1} on a side. Therefore, we measure $\Delta_{\rm F}^2(k)$ over a different range of k values in the open model.

The heavy solid line in each panel of Figure 13 shows results from the PM output with the same linear theory mass fluctuation amplitude as the corresponding TreeSPH simulation. Other lines show $\Delta_{\rm F}^2(k)$ for output times with smaller and larger expansion factors a. We adopt $\Omega = 1$ in the PM simulations, so the amplitude of the linear density fluctuations scales with a. On large scales, the $\Delta_{\rm F}^2(k)$ values from the simulated observations are usually matched by a PM output within $\Delta a = 0.2$ of the correct value, indicating that the normalization procedure recovers the correct amplitude to an accuracy of $\sim 20\%$ or better. To obtain the final normalization for $P(k)$, we take the four $\Delta_{\rm F}^2(k)$ points with $k < 0.015$ (km s^{-1})$^{-1}$ and use linear interpolation among the PM outputs to find the amplitude that best fits that point. We average the four results to obtain the $P(k)$ amplitude and take the scatter between them as an estimate of the normalization error. Analysis of larger volume simulations or a large sample of observational results would warrant a more sophisticated treatment of the amplitude fitting and normalization error.

Figure 14 shows the final product, the normalized estimates of $P(k)$ for the three models. We again plot the results in the directly observable length units, km s^{-1}. Since $P(k)$ has dimensions of length^{-3}, the scaling between h^{-1}Mpc and km s^{-1} affects both the x and y axes. Error bars attached to the individual points represent the 1σ dispersion in $P(k)$ obtained from the five sets of 20 spectra. The error bar in the lower left corner of each panel indicates the uncertainty in

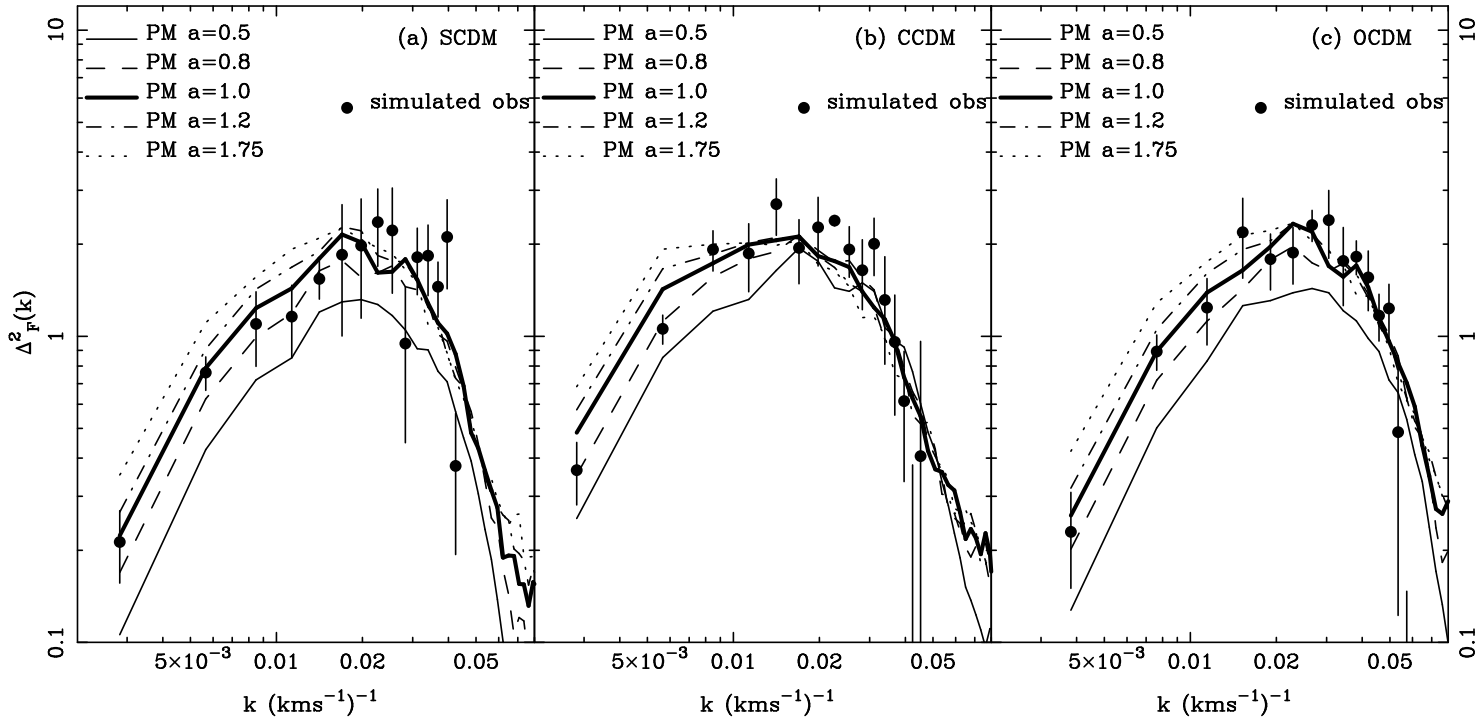

Fig. 13.— Normalization of the recovered $P(k)$ in tests on simulated observations from the (a) SCDM, (b) CCDM, and (c) OCDM models. In each panel, points show $\Delta^2_{\rm F}(k)$ from simulated, continuum–renormalized spectra with S/N=10 and 40 km s^{-1} pixels. Error bars show the 1σ dispersion among five sets of 20 spectra. The heavy solid line shows the average $\Delta^2_{\rm F}(k)$ from four PM simulations with the $P(k)$ obtained from the Gaussianized flux of the simulated data and the same linear theory fluctuation amplitude as the corresponding TreeSPH simulation, i.e., the "correct" normalization. Other lines show $\Delta^2_{\rm F}(k)$ obtained from earlier and later outputs of the PM simulations, corresponding to different linear theory amplitudes proportional to the expansion factor a.

the overall amplitude derived from the normalization procedure; the full set of $P(k)$ points can be coherently shifted up or down by this amount. Solid curves in Figure 14 show the true linear theory power spectra of the three cosmological models.

Figure 14 is the principal result of this paper. It demonstrates that the procedure we have described can recover the correct shape and amplitude of the linear theory mass power spectrum at high redshift, even when it is applied to continuum–fitted spectra with a relatively low signal-to-noise ratio and only moderate spectral resolution.

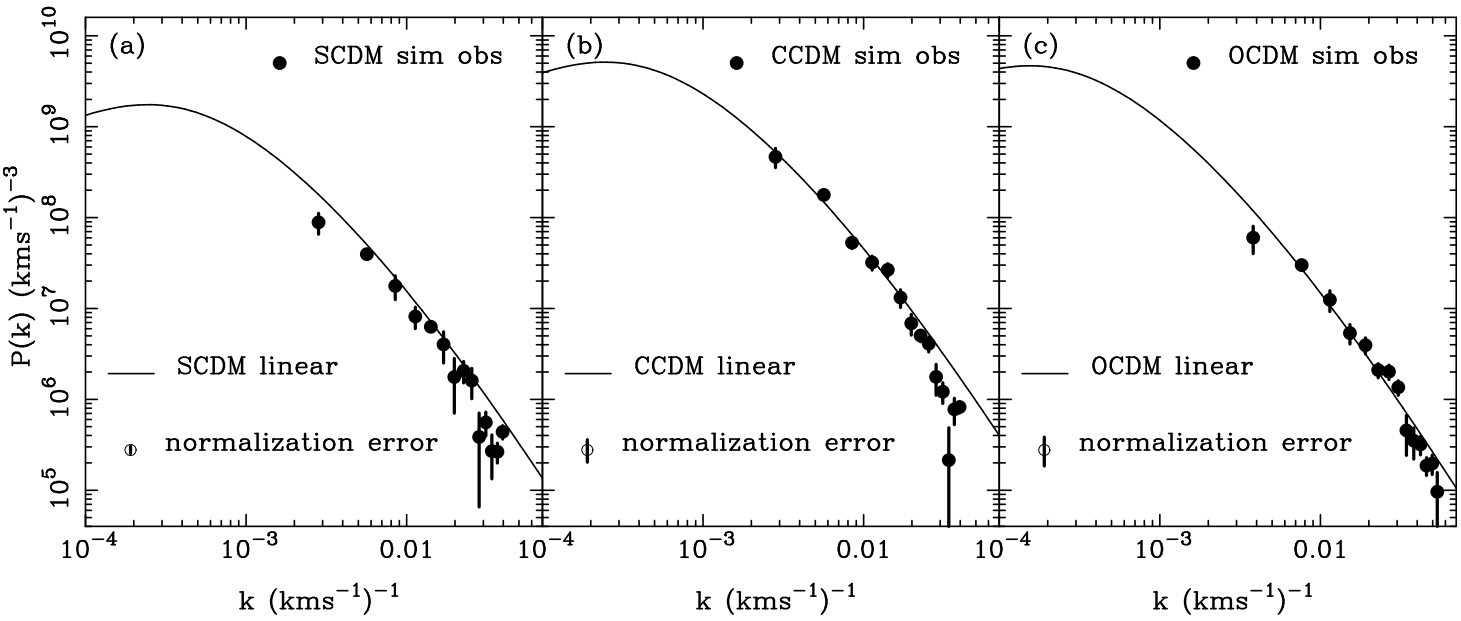

Fig. 14.— Tests of the power spectrum recovery on simulated observations created from the (a) SCDM, (b) CCDM, and (c) OCDM simulations. In each panel, solid curves show the true linear theory mass power spectrum at $z = 3$. Points show $P(k)$ recovered from the Gaussianized flux of the simulated spectra, normalized by matching the flux power spectrum as shown in Fig. 13. Error bars on individual points show the 1σ dispersion among five sets of 20 spectra each. The uncertainty in the overall amplitude resulting from the $\Delta^2_{\rm F}(k)$ fitting is indicated by the "normalization error" in the lower left corner of each panel.

4. Application to the spectrum of Q1422+231

In this Section we present an illustrative application of our $P(k)$ recovery method to a single QSO spectrum. We will analyze larger data sets and carry out more detailed comparisons to the predictions of cosmological models in future work.

We analyze a Keck HIRES spectrum of the QSO Q1422+231 ($z_{\rm QSO} = 3.63$) kindly provided by A. Songaila and L. Cowie. Other analyses of the Lyα forest and associated CIV forest of this QSO spectrum appear in Songaila & Cowie (1996) and Kim et al. (1997). The region of the spectrum between Lyα and Lyβ covers a redshift range $\Delta z \sim 0.7$, over which evolution of the universe has a non-negligible impact. The strongest effect is the changing relation between optical depth and mass overdensity caused by the expansion of the universe and the change in the Hubble expansion rate. For photoionized gas expanding with the Hubble flow in an $\Omega = 1$ universe, the

Lyα optical depth evolves as $(1+z)^{4.5}$ at constant UV background intensity. Following Rauch et al. (1997), we scale the optical depths in the spectrum using this relation to the values they would have at the central redshift of absorption ($z_{\rm abs} = 3.2$). The mean flux decrement that we obtain for this spectrum is $D_A = 0.37$, slightly below the value $D_A = 0.41$ implied by the results of Press et al. (1993). In order to minimize the effect of the evolution in spatial scales, we scale all pixels to the size they would have in km s^{-1} at $z_{\rm abs}$. The maximum resulting change in pixel size is $\sim 10\%$. In practice, this rescaling means that the pixels, which have a constant separation in observed wavelength, are treated as having a constant separation in velocity, $\Delta v = 4$ km s^{-1}. This scaling removes the first-order effect of the expansion of the universe over Δz. Second-order effects due to the change in the Hubble parameter caused by deceleration will remain, but these should be small.

Once we have carried out the above rescalings, we Gaussianize the spectrum and calculate $P(k)$ as described in §2.2. Unlike the simulated spectra, the real spectrum does not have periodic boundaries, so that the 1-dimensional power spectrum we measure by using an FFT is a convolution of the true 1-dimensional power spectrum with a top hat window function that represents the finite length of the QSO spectrum. Because the QSO spectrum is much longer than the largest scale on which we will estimate $P(k)$, the effect of this convolution is negligible. Since we have only a single spectrum, we cannot calculate error bars on $P(k)$ as we did with the ensemble of simulated observations. Instead we split the k range of interest into logarithmically spaced bins, estimate $P(k)$ itself by averaging over the Fourier modes in each bin, and estimate the uncertainty in $P(k)$ from the Poisson errors based on the number of discrete k modes in the bin (i.e., $\Delta P(k) = P(k)/\sqrt{N}$, where N is the number of Fourier modes in the bin).

We use the estimated $P(k)$ to set up the initial density field for the PM code, as described in §2.3. We linearly interpolate between the binned estimates of $P(k)$ to assign power to all k modes in the initial conditions. As in our simulation tests from §3, we generate four different random phase realizations of this initial power spectrum, adopting $\Omega = 1$ and a comoving simulation box size 11.111 h^{-1}Mpc (2222 km s^{-1} at $z = 3$). We evolve the simulations forward so that the scale factor a grows by a factor of 24 in 120 steps of equal Δa. We create artificial spectra with $D_A = 0.37$ at several different output times and measure the flux power spectrum. The resulting values of $\Delta^2_{\rm F}(k)$ are shown in Figure 15, together with $\Delta^2_{\rm F}(k)$ for Q1422+231. In Figure 15 we label the different simulation output times with expansion factors a relative to the expansion factor $a = 1.0$ at which the simulations reproduce the observed $\Delta^2_{\rm F}(k)$. As in §3, we find the normalization of $P(k)$ using the four largest scale points, estimating the amplitude required to match each point by linearly interpolating between the two outputs that bracket the point. We adopt the standard deviation of the four estimates as our estimate of the overall normalization uncertainty. We find that the 1σ error on the amplitude a is 16%. This error does not include the sampling variance that results from the use of only one QSO spectrum, and which could be of comparable magnitude, or even greater. Another source of uncertainty is the value of D_A used in the normalizing simulations. If we had adopted the Press et al. (1993) value of D_A instead of

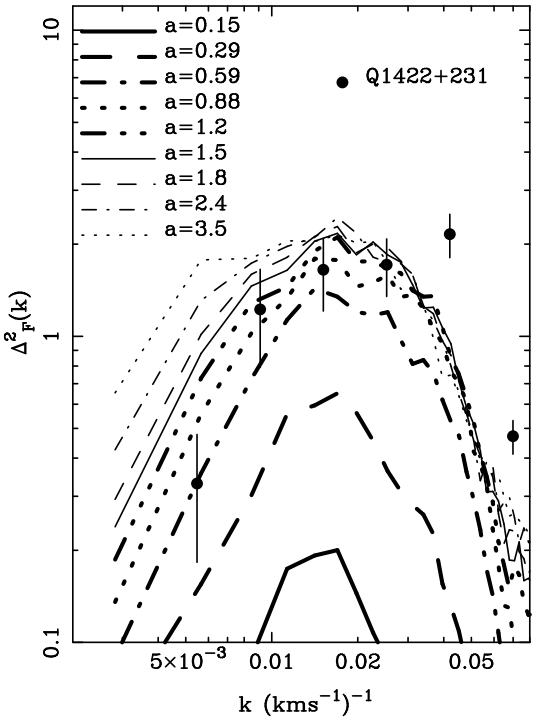

Fig. 15.— Normalization of the mass power spectrum derived from the Lyα forest of Q1422+231. Filled circles show the flux power spectrum for Q1422+231, with error bars computed from Poisson errors in the number of Fourier modes in each logarithmic k bin. Lines show the average flux power spectra from four PM simulations evolved from Gaussian initial conditions with the $P(k)$ shape estimated from this QSO spectrum, at various expansion factors a corresponding to different linear theory mass fluctuation amplitudes. For each of the four lowest k points, we estimate the linear theory amplitude required to match the observed $\Delta^2_{\rm F}(k)$ by linear interpolation between the two bracketing outputs. The $P(k)$ normalization and its uncertainty are determined from the mean and standard deviation of these four estimates.

the mean decrement measured from Q1422+231, then our estimated mass fluctuation amplitude would be lower by $\sim 10\%$ (20% in $P(k)$). On the other hand, as the Zuo & Lu (1993) estimate of D_A is somewhat lower, assuming their value instead would yield a higher amplitude for $P(k)$.

Figure 16 shows the normalized $P(k)$ derived from the spectrum of Q1422+231. The "normalization error" in the lower left corner indicates the uncertainty in the overall amplitude from the normalization procedure, and error bars on individual points are based on Poisson errors in the number of Fourier modes in each k bin. Note that the tests shown in Figure 14 imply that $P(k)$ may be systematically underestimated on the smallest scales, $k \gtrsim 0.025$ (km s^{-1})$^{-1}$.

The curves in Figure 16 show the linear theory power spectra of the SCDM, CCDM, and OCDM models at $z = 3.2$. The shape of the derived $P(k)$ appears to be broadly compatible

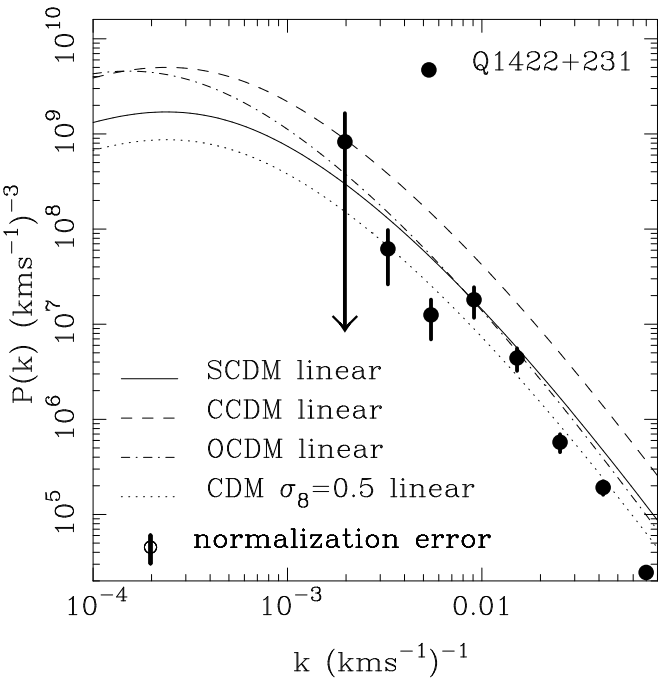

Fig. 16.— The linear mass power spectrum $P(k)$ recovered from the Lyα forest of Q1422+231 (filled circles). Error bars on individual points are computed from the Poisson errors in the number of Fourier modes in each logarithmic k bin. The additional uncertainty in the $P(k)$ normalization, which affects all points coherently, is shown in the lower left corner. Curves show the linear theory power spectra at $z = 3.2$, corresponding to the central absorption wavelength of Q1422+231, for the three CDM models discussed earlier, and for an $\Omega = 1$, $h = 0.5$ CDM model with a lower fluctuation amplitude, corresponding to $\sigma_8 = 0.5$ at $z = 0$.

with the shape predicted for CDM, roughly an $n = -2$ power law on the scales probed by this measurement. The best fit amplitude seems somewhat lower than that in any of our three models, and this difference is seen at large scales where the loss of small-scale power in our tests is negligible. For comparison, we also show the linear theory power spectrum for an $\Omega = 1$, $h = 0.5$ CDM model with a lower amplitude, $\sigma_8 = 0.5$. This model fits the data fairly well over the range of k where the $P(k)$ recovery is reliable. Since Figure 16 is based on a single QSO spectrum, it would be premature to draw strong conclusions about which cosmological models are compatible or incompatible with the data, but it is encouraging that the results derived by our method are roughly in line with theoretical expectations. Comparison to Figure 4 shows that the large scale power detected in the spectrum of Q1422+231 is incompatible with a model in which the Lyα forest is produced by a superposition of unclustered, Voigt-profile lines.

5. Summary and Discussion

We have presented a method for recovering the linear power spectrum of mass fluctuations from QSO Lyα forest spectra. The method is motivated by a simple, approximate description of the relation between Lyα optical depth and underlying mass density in the "fluctuating IGM" scenario for the origin of the Lyα forest. We have carried out extensive tests on artificial QSO spectra created from realistic hydrodynamic cosmological simulations to show that the method successfully recovers both the shape and the amplitude of the mass power spectrum on an interesting range of scales. A preliminary application to the spectrum of Q1422+231 gives results compatible with a low amplitude CDM model.

On small scales, roughly $2\pi/k < 1.5\ h^{-1}$Mpc comoving, our method fails to recover the initial $P(k)$ because of non-linear gravitational evolution and the effective smoothing of the Lyα spectrum produced by peculiar velocities and thermal broadening. Our present investigation does not tell us the largest scale out to which our method can recover $P(k)$; it appears to work from $2\pi/k \sim 1.5\ h^{-1}$Mpc up to the 11.111 h^{-1}Mpc scale of our simulation boxes. There is a hint from the tests in §2.4 that local continuum fitting may artificially suppress power at the largest of these scales, but because our simulations contain only a few modes at this wavelength, it is difficult to tell whether this is a genuine effect or a statistical fluctuation. The continuum–fitting issue requires further investigation with larger volume simulations. For purposes of measuring $P(k)$, techniques that fit a low-order continuum over the largest practical wavelength ranges may be more effective than the conventional fitting technique employed here.

There are other, physical effects that might ultimately limit our ability to measure $P(k)$ on very large scales. One is the inhomogeneity of the UV background intensity (and hence the photoionization rate Γ) due to the finite number of sources (Zuo 1992). Fluctuations in Γ cause fluctuations in the Lyα optical depth that are unconnected to fluctuations in density. The short range of the Lyα forest "proximity effect" relative to the mean separation of QSOs (see, e.g., Bajtlik, Duncan, & Ostriker 1988; Bechtold 1994) implies that fluctuations in Γ are much smaller than unity over most of space, but on large scales the power induced by Γ fluctuations might become comparable to the power in the density field itself. Other subtle effects could become important for $\Delta z \gtrsim 0.2$ ($2\pi/k \gtrsim 60,000[1+z]^{-1}$ km s^{-1}), such as evolution of the UV background and evolution of the density field itself.

Our method explicitly incorporates the assumption that primordial fluctuations are Gaussian, as predicted in most inflationary models. Figure 2 suggests that the recovered *shape* of $P(k)$ is not particularly sensitive to this assumption; Gaussianization is a useful, theoretically motivated tool for "regularizing" the observed absorption and thus reducing statistical fluctuations in the $P(k)$ estimates, but because non-linear local transformations do not alter the shape of the power spectrum at large scales, we obtain a similar average $P(k)$ from our simulated spectra whether or not we Gaussianize the flux. We rely more heavily on the Gaussian assumption when we normalize $P(k)$, since we employ PM simulations with random phase initial conditions. Because we use

the flux power spectrum, a variance measure, as our criterion for normalizing $P(k)$, we might obtain similar results even for other assumptions, but the sensitivity of the normalization to the Gaussian assumption can only be assessed quantitatively in the context of a more explicit model for non-Gaussian primordial fluctuations.

The recovery of the mass power spectrum relies more generally on the theoretical scenario for the Lyα forest provided by cosmological simulations and outlined in §2.1. Lyα forest observations also provide the means to test this scenario, and to test the assumption of Gaussian fluctuations, especially once the range of cosmological models to be considered is narrowed by the $P(k)$ determination. Traditional measures based on line-fitting, such as the column density and b-parameter distributions, provide one class of important tests. Statistical methods that treat the spectrum as a continuous field rather than a superposition of lines may ultimately prove more powerful, since they are tied more directly to the quantities observed and are better attuned to the physics of a continuous, fluctuating IGM (see, e.g., Miralda-Escudé et al. 1996; Croft et al. 1997b; Rauch et al. 1997; Weinberg et al., in preparation). Observations of absorption along neighboring lines of sight probed by QSO pairs and groups can also provide crucial tests, by constraining the sizes and geometry of the absorbing structures (Bechtold et al. 1994; Dinshaw et al. 1994; Dinshaw et al. 1995; Crotts & Fang 1997).

Within the broad context of inflationary models for structure formation, "free" parameters include Ω_0, Λ_0, h, Ω_b, the neutrino density parameter Ω_ν (with the implied cold dark matter density parameter $\Omega_c = \Omega_0 - \Omega_\nu - \Omega_b$), the primeval spectral index n, the ratio of tensor-to-scalar contributions to large angle CMB anisotropies, and the energy density of the relativistic particle background (from CMB photons and light neutrinos, for example). Particular regions within this parameter space are often identified as named models, such as mixed dark matter, ΛCDM, open CDM, or tilted CDM. These models resolve the observational conflicts that beset the most "natural" inflation model ($\Omega_0 = 1$, $n = 1$, etc.) by appealing to different variations of the fundamental physics — e.g., by adjusting the matter content, the vacuum energy, the space geometry, or the inflaton potential. In combination with existing observational constraints from CMB anisotropies and large scale structure, precise measurements of the shape and amplitude of $P(k)$ at $z \sim 2 - 4$ can rapidly shrink the viable regions of parameter space and thus rule out or severely restrict many of these conceptually distinct models. These measurements even have the potential to rule out the general inflationary, adiabatic fluctuation scenario for the origin of structure by revealing a radically different $P(k)$, though our results from Q1422+231 suggest that they will not.

The $P(k)$ constraints from the Lyα forest complement the observational constraints from the CMB and large scale structure because they probe epochs between recombination and the present day and because they respond differently to parameter variations. Consider, for example, the CCDM model, which appears at least marginally incompatible with the $P(k)$ inferred from Q1422+231 (Figure 16). It is well known that the CCDM model is incompatible with the observed virial masses of rich galaxy clusters, because it combines $\Omega_0 = 1$ with a high value of σ_8 (see, e.g.,

White et al. 1993). However, our $P(k)$ measurement challenges this model on different grounds, and the challenge would also apply to a low-Ω_0 model that has the same $P(k)$ amplitude at $z = 3$, even though such a model might pass the cluster test. A difference from large scale structure constraints also arises because the directly observable "length" units for Lyα forest studies are km s^{-1}, and the relation of these scales to h^{-1}Mpc at $z = 0$ depends on the time evolution of the Hubble expansion rate, and hence on Ω_0 and Λ_0. The constraints from the Lyα forest $P(k)$ will be especially powerful if they can be extended to redshifts low enough that the fluctuation growth rate and the redshift dependence of $H(z)$ start to differ measurably from one cosmological model to another. Since our tests indicate that high spectral resolution and high signal-to-noise ratio are not essential, the data from the HST Absorption Line Key Project (Bahcall et al. 1993; Jannuzi et al. 1997) and other HST studies of the low-z Lyα forest may well be adequate for this purpose. The critical questions are whether the relation between Lyα optical depth and mass density remains sufficiently tight as the universe evolves and whether large scale fluctuations remain measurable with the much lower mean absorption observed at low redshift (reflecting the lower value of A in equation [2]). High resolution hydrodynamic simulations evolved to $z = 0$ should soon provide the means to answer these questions.

The prospects for determining $P(k)$ at $z = 2 - 4$ with existing QSO absorption data are excellent. (At $z = 4$, continuum determination may be a significant obstacle because of the high mean opacity.) There are already numerous Keck HIRES spectra comparable in quality to the Q1422+231 spectrum that we have analyzed here. Furthermore, our tests show that spectra of moderate resolution and signal-to-noise ratio are adequate for $P(k)$ determinations, and since one wants as many spectra as possible in order to beat down cosmic variance and achieve high statistical precision over a range of redshifts, the large existing samples of "pre-Keck" spectra (e.g., Bechtold 1994) may be even better suited to this purpose. For future programs designed specifically for power spectrum studies, observations targeting groups of QSOs with transverse separations of several to several 10's of comoving h^{-1}Mpc (e.g., Williger et al. 1996) might be especially valuable, as cross-correlating spectra along parallel lines of sight rapidly multiplies the number of baselines available for estimating $P(k)$. With a sufficiently large sample, one could even use the angular dependence of $P(k)$ to constrain spacetime geometry (Alcock & Paczyński 1979; Matsubara & Suto 1996; Ballinger, Peacock, & Heavens 1997; Popowski et al. 1997). The Sloan Digital Sky Survey, which will obtain $\sim 10^5$ QSO spectra with 2.5$\AA$ resolution and typical S/N$\sim 10 - 20$, may eventually provide the ideal data set for such a study.

The promise of the method described in this paper arises from the happy coincidence between the excellent observational data on the Lyα forest and the simple physical interpretation of these data that has emerged from cosmological simulations. Because the Lyα forest arises primarily in the diffuse, smoothly fluctuating IGM, this route to $P(k)$ sidesteps the uncertainties in theoretical modeling of galactic star formation, feedback, galaxy mergers, and so forth, which inevitably affect interpretations of large scale structure data. Determination of the mass power spectrum in the high redshift universe now looks to be within relatively easy reach.

We thank A. Songaila and L. Cowie for providing the Q1422+231 spectrum and J. Miralda-Escudé for helpful discussions and for the program used to generate the Voigt-profile line model used in Figure 4. This work was supported by NASA Astrophysical Theory Grants NAG5-2864, NAG5-3111, NAGW-2422, NAG5-2793, and NAG5-3922, by NASA Long-Term Space Astrophysics Grant NAG5-3525, and by the NSF under grants ASC93-18185 and the Presidential Faculty Fellows Program. The SPH simulations were performed at the San Diego Supercomputer Center.

REFERENCES

Alcock, C., & Paczyński, B. 1979, Nature, 281, 358

Bahcall, J. N., et al. 1993, ApJS, 87, 1

Bajtlik, S., Duncan, R.C., & Ostriker, J.P. 1988, ApJ, 327, 570

Ballinger, W. E., Peacock, J. A., & Heavens, A. F. 1997, MNRAS, in press (astro-ph/9605017)

Baugh, C. M. 1996, MNRAS, 282, 1413

Bechtold, J. 1994, ApJS, 91, 1

Bechtold, J., Crotts, A. P. S., Duncan, R. C., & Fang, Y. 1994, ApJ, 437, L83

Bennett, C. L., Banday, A. J., Gorskí, K. M., Hinshaw, G., Jackson, P., Keegstra, P., Kogut, A., Smoot, G. F., Wilkinson, D. T., & Wright, E. L. 1996, ApJ, 646, L1

Bi, H.G. 1993, ApJ, 405, 479

Bi, H.G. & Davidsen, A. 1997, ApJ, 479, 523

Bi, H., Ge, J., & Fang, L.-Z. 1995, ApJ, 452, 90

Cen, R., Miralda-Escudé, J., Ostriker, J.P., & Rauch, M. 1994, ApJ,437, L9

Coles, P., & Jones, B. J. T. 1991, MNRAS, 248, 1

Cristiani, S., D'Odorico, S., D'Odorico, V., Fontana, A., Giallongo, E., & Savaglio, S. 1997, MNRAS, 285, 209

Croft, R. A. C., Weinberg, D. H., Hernquist, L., & Katz, N. 1997b, in Proceedings of the 18th Texas Symposium on Relativistic Astrophysics, eds. A. Olinto, J. Frieman, & D. Schramm, (Singapore: World Scientific), in press (astro-ph 9701166)

Croft, R.A.C., Weinberg, D.H., Katz, N., & Hernquist, L. 1997a, ApJ, in press (astro-ph/9611053)

Crotts, A. P. S., & Fang, Y. 1997, ApJ, submitted (astro-ph/9702185)

Davé, R., Hernquist, L., Weinberg, D. H., & Katz, N. 1997, ApJ, 477, 21

Dinshaw, N., Impey, C. D., Foltz, C. B., Weymann, R. J., & Chaffee, F. H. 1994, ApJ, 437, L87

Dinshaw, N., Foltz, C. B., Impey, C. D., Weymann, R. J., & Morris, S. L. 1995, Nature, 373, 223

Gnedin, N. Y. 1997, MNRAS, submitted (astro-ph/9706286)

Gnedin, N. Y., & Hui, L. 1996, ApJ, 472, L73

Gnedin, N. Y., & Hui, L. 1997, MNRAS, submitted (astro-ph/9706219)

Gunn, J.E., & Peterson, B.A. 1965, ApJ, 142, 1633

Hamilton, A. J. S., Matthews, A., Kumar, P., & Lu, E. 1991, ApJ, 374, L1

Heisler, J., Hogan, C. J., & White, S. D. M. 1989, ApJ, 347, 52

Hernquist, L., & Katz, N. 1989, ApJS, 70, 419

Hernquist L., Katz N., Weinberg D.H., & Miralda-Escudé J. 1996, ApJ, 457, L5

Hockney, R. W., & Eastwood, J. W. 1981, Computer Simulations Using Particles, (New York: McGraw Hill)

Hu, E.M., Kim, T.S., Cowie, L.L., Songaila, A., & Rauch, M. 1995, AJ, 110, 1526

Hui, L., & Gnedin, N. 1997, MNRAS, submitted (astro-ph/9612232)

Hui, L., Gnedin, N., & Zhang, Y. 1997, ApJ, in press (astro-ph/9608157)

Jain, B., Mo, H. J., & White, S. D. M. 1995, MNRAS, 276, L25

Jannuzi, B., et al. 1997, ApJS, submitted

Kaiser, N. 1987, MNRAS, 227, 1

Kaiser, N., & Peacock, J. A. 1991, ApJ, 379, 482

Katz, N., Weinberg D.H., & Hernquist, L. 1996, ApJS, 105, 19

Kim, T. S., Hu, E. M., Cowie, L. L., & Songaila, A. 1997, AJ, in press (astro-ph/9704184)

Matsubara, T., & Suto, Y. 1996, ApJ, 470, L1

Miralda-Escudé J., Cen R., Ostriker J.P., & Rauch M. 1996, ApJ, 471, 582

Mücket, J. P., Petitjean, P., Kates, R. E., & Riediger, R. 1996, A&A, 308, 17

Nusser, A., & Colberg, J. M. 1997, MNRAS, submitted (astro-ph/9705121)

Pando, J., & Fang, L. 1995, ApJ, submitted (astro-ph/9509032)

Peacock, J. A., & Dodds, S. J. 1996, MNRAS, 280, L19

Peebles, P. J. E. 1980, The Large Scale Structure of the Universe (Princeton: Princeton University Press)

Petitjean, P., Mücket, J. P., & Kates, R. E. 1995, A&A, 295, L9

Popowski, P. A., Weinberg, D. H., Ryden, B. S., & Osmer, P. S. 1997, ApJ, submitted (astro-ph/9707175)

Press W. H., & Rybicki G. B. 1993, ApJ, 414, 64

Press W.H., Rybicki G.B., & Schneider D.P. 1993, ApJ, 414, 64

Quashnock, J. M., Vanden Berk, D. E., & York, D. G. 1996, ApJ472, L69

Quashnock, J. M., & Vanden Berk, D. E. 1997, ApJ, submitted (astro-ph/9706233)

Ratra, B., Sugiyama, N., Banday, A. J., & Gorskí, K. M. 1997, ApJ, 481, 22

Rauch, M., Miralda-Escudé, J., Sargent, W. L. W., Barlow, T. A., Weinberg, D. H., Hernquist, L., Katz, N., Cen, R., & Ostriker, J. P. 1997, ApJ, in press, astro-ph/9612245

Reisenegger, A., & Miralda-Escudé, J. 1995, ApJ, 449, 476

Sargent, W. L. W., Boksenberg, A., & Steidel, C. C. 1989, ApJS, 68, 539

Songaila, A., & Cowie, L.L. 1996, AJ, 112, 335

Wadsley, J. W., & Bond, J.R. 1996, in Proc. 12th Kingston Conference, Computational Astrophysics, eds. D. Clarke & M. West (San Francisco: ASP Conference Series), in press (astro-ph/9612148)

Walker, T.P., Steigman, G., Schramm, D.N., Olive, K.A., & Kang, H.S 1991, ApJ, 376, 51

Weinberg, D. H. 1992, MNRAS, 254, 315

Weinberg, D. H. 1995, in Wide-Field Spectroscopy and the Distant Universe, eds. S. J. Maddox & A. Aragón-Salamanca (Singapore: World Scientific), 129

Weinberg, D. H., & Gunn, J. E. 1990, ApJ, 352, L25

White, S. D. M., Efstathiou, G. P., & Frenk, C. S. 1993, MNRAS, 262, 1023

Williger, G. M., Hazard, C., Baldwin, J. A., & McMahon, R. G. 1996, ApJS, 104, 145

Zel'dovich, Y. B. 1970, A&A, 5, 84

Zhang Y., Anninos P., & Norman M.L. 1995, ApJ, 453, L57

Zuo, L. 1992, MNRAS, 258, 36

Zuo, L. & Bond, J. R. 1994, ApJ, 423, 73

Zuo, L. & Lu, L. 1993, ApJ, 418, 601